


## Review

# Repurposing Mining and Metallurgical Waste as Electroactive Materials for Advanced Energy Applications: Advances and Perspectives

Fenghui Guo <sup>1,2</sup>, Qian Chen <sup>3</sup>, Zhihao Liu <sup>4</sup> , Dongle Cheng <sup>3,5,6</sup>, Ning Han <sup>7</sup>  and Zhijie Chen <sup>3,\*</sup> <sup>1</sup> College of Earth Sciences, Guilin University of Technology, Guilin 541006, China<sup>2</sup> Shenzhen Academy of Metrology and Quality Inspection, Shenzhen 518000, China<sup>3</sup> Centre for Technology in Water and Wastewater, School of Civil and Environmental Engineering, University of Technology Sydney, Sydney, NSW 2007, Australia<sup>4</sup> Department of Environmental Science, School of Environment and Ecology, Chongqing University, Chongqing 400045, China<sup>5</sup> College of Safety and Environmental Engineering, Shandong University of Science and Technology, Qingdao 266590, China<sup>6</sup> Institute of Yellow River Delta Earth Surface Processes and Ecological Integrity, Shandong University of Science and Technology, Qingdao 266590, China<sup>7</sup> Department of Materials Engineering, KU Leuven, 3001 Leuven, Belgium

\* Correspondence: zhijie.chen@uts.edu.au

**Abstract:** Developing cost-effective electroactive materials for advanced energy devices is vital for the sustainable development of electrochemical energy conversion/storage systems. To reduce the fabrication cost of electroactive materials (electrocatalysts and electrodes), growing attention has been paid to low-cost precursors. Recently, mining and metallurgical waste has been used to design electroactive materials, which shows great economic and environmental benefits. Herein, current achievements in the applications of mining and metallurgical waste-derived electroactive materials in sustainable energy conversion/storage fields (batteries, supercapacitors, fuel cells, and small-molecule electro-conversion) are comprehensively analyzed. The waste-to-materials conversion methods and materials' structure–performance relationships are emphasized. In addition, perspectives related to the further development and applications of waste-derived high-performance electroactive materials are pointed out.

**Keywords:** waste utilization; electrocatalysts; green chemistry; batteries; supercapacitors; fuel cells; energy storage; energy conversion



**Citation:** Guo, F.; Chen, Q.; Liu, Z.; Cheng, D.; Han, N.; Chen, Z. Repurposing Mining and Metallurgical Waste as Electroactive Materials for Advanced Energy Applications: Advances and Perspectives. *Catalysts* **2023**, *13*, 1241. <https://doi.org/10.3390/catal13091241>

Academic Editor: Carlo Santoro

Received: 6 August 2023

Revised: 21 August 2023

Accepted: 25 August 2023

Published: 26 August 2023



**Copyright:** © 2023 by the authors. Licensee MDPI, Basel, Switzerland. This article is an open access article distributed under the terms and conditions of the Creative Commons Attribution (CC BY) license (<https://creativecommons.org/licenses/by/4.0/>).

## 1. Introduction

The global mining and metallurgical industries which provide raw materials for diverse sectors play a critical role in the development of our modern society. Mining and metallurgical activities are highly pollution-intensive, and gaseous, solid, and liquid pollutants are generally produced from the related processing systems [1]. In particular, mining and metallurgical wastes, like metallurgical slags, mine tailings/gangues, ore residues, electroplating sludge, red mud, and metal-rich wastewater/leachates, can pose a serious stress on the surrounding water and soil environments due to their huge amounts and complex physicochemical properties [2–4]. As reported, over 7 billion tons of mine tailings are generated yearly, globally, and 19 billion solid tailings will be accumulated by 2025 [5]. In this context, rationally handling mining and metallurgical waste is an urgent mission. Current studies suggest that mining and metallurgical waste can be directly used as construction materials [4], and physical beneficiation process and hydrometallurgical and pyrometallurgical methods also have been employed in the recycling/reuse of mining and metallurgical waste [6]. Importantly, most current mining and metallurgical waste is

rich in metals, and the utilization of such valuable components in mining and metallurgical waste has become a hotspot due to the potential environmental and economic benefits.

Researchers find that general elements (e.g., Fe, Cu, V, Ni, Co, Sn, Ti, Mn, and Si) in most mining and metallurgical waste are widely employed in the design of electroactive materials for advanced energy applications [7–11]. For example, Ni-based materials are extensively used in supercapacitors [12,13], and Fe/Ni/Co-based materials are active for the electrodes of batteries [14,15] and water splitting [16,17]. In this context, using mining and metallurgical waste precursors to develop electroactive materials can significantly promote the utilization of hazardous waste, lessen the negative eco-impacts of waste, and cut the cost of electroactive materials. Following the circular economy principle, diverse mining and metallurgical wastes have been recently employed for constructing effective electroactive materials for sustainable energy storage/conversion systems, including rechargeable batteries [18], supercapacitors [19], fuel cells [20], water electrolysis [21], and other small-molecule conversions [22]. For example, Liu and coauthors found that red mud could be used as an efficient anode material for Li-ion batteries (a high discharge/charge capacity of  $1668.1 \text{ mAh} \cdot \text{g}^{-1}$  at  $0.1 \text{ A} \cdot \text{g}^{-1}$  after 200 cycles) via an acid pretreatment–hydrothermal process method [23]. By integrating these waste-based materials into advanced electrochemical applications, the “waste-to-value” practice significantly promotes the sustainable development of energy systems. However, a comprehensive review on the recent advances in the utilization of mining and metallurgical waste-based electroactive materials in electrochemical energy applications remains unavailable.

Herein, we thoroughly analyze current achievements in the applications of mining and metallurgical waste-derived electroactive materials in sustainable energy conversion/storage fields, e.g., batteries, supercapacitors, fuel cells, and small-molecule electroconversion. We emphasize the strategies for performance optimization of electroactive materials, and materials’ structure–performance relationships are also illustrated. In addition, perspectives in the rapidly developing field are presented for guiding future circular economy-driven sustainable energy applications.

## 2. Mining and Metallurgical Waste-Based Electroactive Materials for Advanced Energy Applications

Electrochemical energy storage and conversion techniques are highly important to replace current fossil-fuel-based energy systems, with the ambitious goal to decarbonize the global energy sector. Currently, rechargeable batteries, supercapacitors, fuel cells, and energy-related electro-conversion of small-molecule (e.g.,  $\text{CO}_2$ ,  $\text{H}_2\text{O}$ , and  $\text{NH}_3$ ) systems have shown practical applications on a large scale. To reduce the system running costs, many efforts have been made to use low-cost electrodes and electrocatalysts. Mining and metallurgical waste-based materials have thus been widely applied in these advanced energy systems in recent years, as shown in Table 1. In this section, the utilization of mining and metallurgical waste-based electroactive materials in advanced energy systems is discussed, and methods to improve the material performance are emphasized.

**Table 1.** A summary of representative mining and metallurgical waste-based electroactive materials for advanced energy applications.

Material	Waste	Synthesis Method	Application	Performance
Si/TiSi <sub>2</sub> [24]	Ti-bearing blast furnace slag	Induction melting–mechanical ball milling	LIBs <sup>1</sup>	Reversible capacity: $530 \text{ mAh} \cdot \text{g}^{-1}$ (after 200 cycles at $0.8 \text{ A} \cdot \text{g}^{-1}$ )
NiFe <sub>2</sub> O <sub>4</sub> [25]	Electroplating sludge	Hydrothermal process–acid washing	LIBs	Reversible capacity: $316.94 \text{ mAh} \cdot \text{g}^{-1}$ (at $0.5 \text{ A} \cdot \text{g}^{-1}$ )
Mesoporous silicon [26]	Iron slag	Acid leaching–magnesiothermic reaction	LIBs	Reversible capacity: $1566 \text{ mAh} \cdot \text{g}^{-1}$ (after 30 cycles at $1 \text{ A} \cdot \text{g}^{-1}$ )

Table 1. Cont.

Material	Waste	Synthesis Method	Application	Performance
MoO <sub>2</sub> @coal gangue [27]	Coal gangue	Acid leaching–hydrothermal process	LOBs <sup>2</sup>	Initial discharge capacity: 9748 mAh·g <sup>−1</sup>
Multi-doped LiFePO <sub>4</sub> /C [28]	Steel slag	Roasting–carbothermic reduction	LIBs	Capacity: 117 mAh·g <sup>−1</sup> (at 0.15 A·g <sup>−1</sup> )
Cation-intercalated V <sub>2</sub> O <sub>5</sub> ·nH <sub>2</sub> O [29]	Vanadium slag	Roasting–leaching–hydrothermal process	AZIBs <sup>3</sup>	Capability: 317 mAh g <sup>−1</sup> (after 4000 cycles at 20 A·g <sup>−1</sup> )
Fe <sub>2</sub> O <sub>3</sub> [19]	Vanadium titanomagnetite tailings	Alkali fusion–hydrothermal process–pyrolysis	Supercapacitors	Capacitance: 151.5 F·g <sup>−1</sup> at 1 A·g <sup>−1</sup> (NiCo(O)S//Fe <sub>2</sub> O <sub>3</sub> ASC <sup>4</sup> )
Metal-doped carbon [30]	Metallurgical slag	Pyrolysis	Supercapacitors	Capacitance: 135 F·g <sup>−1</sup> at 0.5 A·g <sup>−1</sup>
β-Ni(OH) <sub>2</sub> [31]	Electroless nickel plating bath	Precipitation	Supercapacitors	Energy density: 11.5 W·h·kg <sup>−1</sup> , power density: 207.5 W·kg <sup>−1</sup>
Amorphous Ni(HCO <sub>3</sub> ) <sub>2</sub> [12]	Nickel-containing electroplating sludge	Hydrothermal method	Supercapacitors	Capacitance: 599.8 C·g <sup>−1</sup> at 1 A·g <sup>−1</sup>
Barium slag-derived catalyst [32]	Barium slag	Precipitation–heating	DC-SOFCs <sup>5</sup>	Power: 249 mW·cm <sup>−2</sup>
Goethite [20]	Mining mud	Precipitation	MFCs <sup>6</sup>	Power: 17.1 W·m <sup>−3</sup> at 20 Ω
Sn@N/P-doped carbon [22]	Electroplating sludge	Annealing	CO <sub>2</sub> RR <sup>7</sup>	FE <sup>8</sup> for HCOOH: 87.93% at −1.05 V vs. RHE <sup>9</sup>
CuPb electrocatalyst [33]	Fayalite slag	Chemical extraction–electrodeposition	CO <sub>2</sub> RR	FE for CO: 41.1% at −1.05 V vs. RHE
Metal-doped CuCr <sub>2</sub> O <sub>4</sub> [34]	Electroplating sludge	Calcination	N <sub>2</sub> RR <sup>10</sup>	Ammonia yield: 15.9 μg·h <sup>−1</sup> mg <sup>−1</sup> <sub>cat</sub>
Red mud [35]	Red mud	Ball milling	NO <sub>3</sub> RR <sup>11</sup>	Ammonia yield: 0.16 mmol cm <sup>−2</sup> h <sup>−1</sup> at −0.73 V vs. RHE
FeNiCuSnB [21]	Hydrometallurgical wastewater	Boriding	OER <sup>12</sup>	η <sub>10</sub> <sup>13</sup> : 199 mV, Tafel slope: 53.98 mV·dec <sup>−1</sup>

Note: <sup>1</sup> LIBs: lithium-ion batteries; <sup>2</sup> LOBs: Li-O<sub>2</sub> batteries; <sup>3</sup> AZIBs: aqueous Zn-ion batteries; <sup>4</sup> ASC: asymmetric supercapacitor; <sup>5</sup> DC-SOFCs: direct carbon solid oxide fuel cells; <sup>6</sup> MFCs: microbial fuel cells; <sup>7</sup> CO<sub>2</sub>RR: CO<sub>2</sub> reduction reaction; <sup>8</sup> FE: Faradic efficiency; <sup>9</sup> RHE: reversible hydrogen electrode; <sup>10</sup> N<sub>2</sub>RR: N<sub>2</sub> reduction reaction; <sup>11</sup> NO<sub>3</sub>RR: NO<sub>3</sub><sup>−</sup> reduction reaction; <sup>12</sup> OER: oxygen evolution reaction; <sup>13</sup> η<sub>10</sub>: overpotential at the current density of 10 mA cm<sup>−2</sup>.

## 2.1. Batteries

### 2.1.1. Anode Materials

Rechargeable batteries with eco-friendliness, high energy density, and long cycling stability have already been extensively employed in portable electronics, electric vehicles, and grid energy storage [36,37]. In batteries, electrodes (anodes and cathodes) are critical components that govern the working performance [38,39]. For anodes, materials with high energy density, high power density, and good cycling stability are required. Anodes based on carbon group elements (C, Si, and Sn) and transition metal (e.g., Fe and Ni) oxides have been successfully developed from mining and metallurgical waste. Carbon materials, like graphene and its analogues, are traditional anode materials for rechargeable batteries, especially LIBs. However, the relatively low Li<sup>+</sup> transfer efficiency limits their practical applications. To address this problem, studies have focused on composite materials. For instance, starting from graphite tailings and coking coal, Fu and coauthors developed a carbon-based composite by one-step pyrolysis [40]. With a lamellar structure, enhanced isotropy, and rich N and S dopants, the composite has a high Li<sup>+</sup> diffusion coefficient ( $6.26 \times 10^{-10}$ – $171 \times 10^{-10}$  cm<sup>2</sup>·s<sup>−1</sup>) under the charging state.

Si anodes have the merit of higher theoretical specific capacity than graphite (4200 vs. 372 mAh·g<sup>−1</sup>), and thus growing attention has been paid to developing earth-abundant

Si-based anode materials [41,42]. Current efforts emphasize the nanostructure design and composite construction. Chun and coauthors fabricated a highly mesoporous silicon (Porous-Si<sub>slag</sub>) from waste iron slag (Figure 1a) [26]. The scanning electron microscopy (SEM) images show that Porous-Si<sub>slag</sub> possesses a rough surface and consists of interconnected nanoparticles with small size (<30 nm) (Figure 1b,c), and it has a specific surface area (SSA) of 438 m<sup>2</sup>·g<sup>−1</sup>. Also, rich pores can be identified in the structure. These structural properties benefit the exposure of a large electroactive surface area and strengthen the resistance to structural deformation during the charge/discharge process. As such, Porous-Si<sub>slag</sub> exhibits higher rate capability and cycle stability than commercial Si-based analogues (Figure 1d,e). Si-based composites from mining and metallurgical waste also show high performance as anodes for LIBs, such as waste vermiculite-derived Si/C [43], coal gangue-based hierarchical porous C/SiO<sub>x</sub> [44], and blast furnace slag-derived Si/TiSi<sub>2</sub> [24]. The combination of two components can not only enhance the electrochemical activities but also alleviate volume change of anodes during cycling. Sn-based materials are also promising anodes for practical batteries for their relatively high theoretical capacity (992 mAh·g<sup>−1</sup>) and good operating safety [45]. Rich in Sn, electroplating sludge can be converted into the Sn@C composite via a bacteria-involved process (Figure 1f) [46]. In the rod-shaped Sn@C composite, Sn nanoparticles are evenly distributed on the carbon without obvious agglomeration (Figure 1g–i). Further electrochemical tests indicate that the Sn@C composite has a Coulombic efficiency (CE) of 70.3% and a high reversible capacity of 297 mAh·g<sup>−1</sup> at 10 A·g<sup>−1</sup> (Figure 1j). Also, the Sn@C composite exhibits a good long-term cyclic stability for 1500 cycles at 1 A·g<sup>−1</sup> (Figure 1k).

Earth-abundant transition metal-based oxide (TMO) materials have high theoretical capacities of 600–1200 mAh g<sup>−1</sup>, as the anode materials of LIBs [47]. Together with their good thermal/chemical stability, facile preparation, and low cost [48], mining and metallurgical waste-derived TMOs are favorable choices for anode materials. By a facile chemical precipitation process, α-Fe<sub>2</sub>O<sub>3</sub> nanoparticles can be obtained from the leaching liquor of tin ore tailings [18]. Interestingly, the choice of precipitants has a prominent impact on the electrochemical performance of α-Fe<sub>2</sub>O<sub>3</sub> products. Compared with sodium hydroxide and ammonia, the utilization of sodium carbonate leads to a more active anode material, which may be due to the formation of interconnected structures. The optimal one shows a high reversible discharge capacity over 1100 mAh·g<sup>−1</sup> after 300 cycles at 0.5 A·g<sup>−1</sup>. Further analysis suggests that pseudocapacitance largely contributes to Li<sup>+</sup> storage in α-Fe<sub>2</sub>O<sub>3</sub>. γ-Fe<sub>2</sub>O<sub>3</sub> also exhibits good electrochemical performance as an LIB anode material. Suryawanshi et al. extracted a composite oxide material (γ-Fe<sub>2</sub>O<sub>3</sub> major phase with inter-dispersed Ti/Si/Al oxides) from red mud via a magnetic separation process (Figure 2a) [49]. The full cell assembled with the γ-Fe<sub>2</sub>O<sub>3</sub> anode and LiMn<sub>2</sub>O<sub>4</sub> cathode has high power capability, good capacity retention, and long-term cyclability features, as displayed in Figure 2b,c. It has been found that γ-Fe<sub>2</sub>O<sub>3</sub> is responsible for the high activities, while those inactive oxides (Fe<sub>2</sub>TiO<sub>4</sub>, SiO<sub>2</sub>, and Al<sub>2</sub>O<sub>3</sub>) could help to sustain the stability of the anode by alleviating the electrode volume expansion during the charge/discharge process. The critical role of such inactive components in anodes is also supported by Liu and coworkers, who developed a α-Fe<sub>2</sub>O<sub>3</sub> phase-dominant anode material from red mud with an acid pretreatment–hydrothermal method [23]. To enhance the electrochemical performance of monometal oxides, introducing a second active metal to form mixed metal oxides is recommended. Weng et al. constructed a NiFe<sub>2</sub>O<sub>4</sub> anode material from electroplating sludge with a two-step hydrothermal treatment–acid-washing method (Figure 2d) [25]. The X-ray diffraction (XRD) pattern of the final product shows a high proportion of NiFe<sub>2</sub>O<sub>4</sub> phase (Figure 2e), and little amounts of other metal (e.g., Cu and Cr) oxides also exist in the solid. The NiFe<sub>2</sub>O<sub>4</sub> product is in the form of nano-spherical particles with a small diameter (<100 nm) (Figure 2f). Interestingly, the NiFe<sub>2</sub>O<sub>4</sub> anode has a CE of 67.81%, and it exhibits a high reversible capacity of 513.15 mAh·g<sup>−1</sup> at 0.1 A·g<sup>−1</sup> (Figure 2g,h). Although the Fe precursor is additionally added for the formation of Ni-Fe oxides, this study provides a feasible way to utilize multi-metal complex waste.

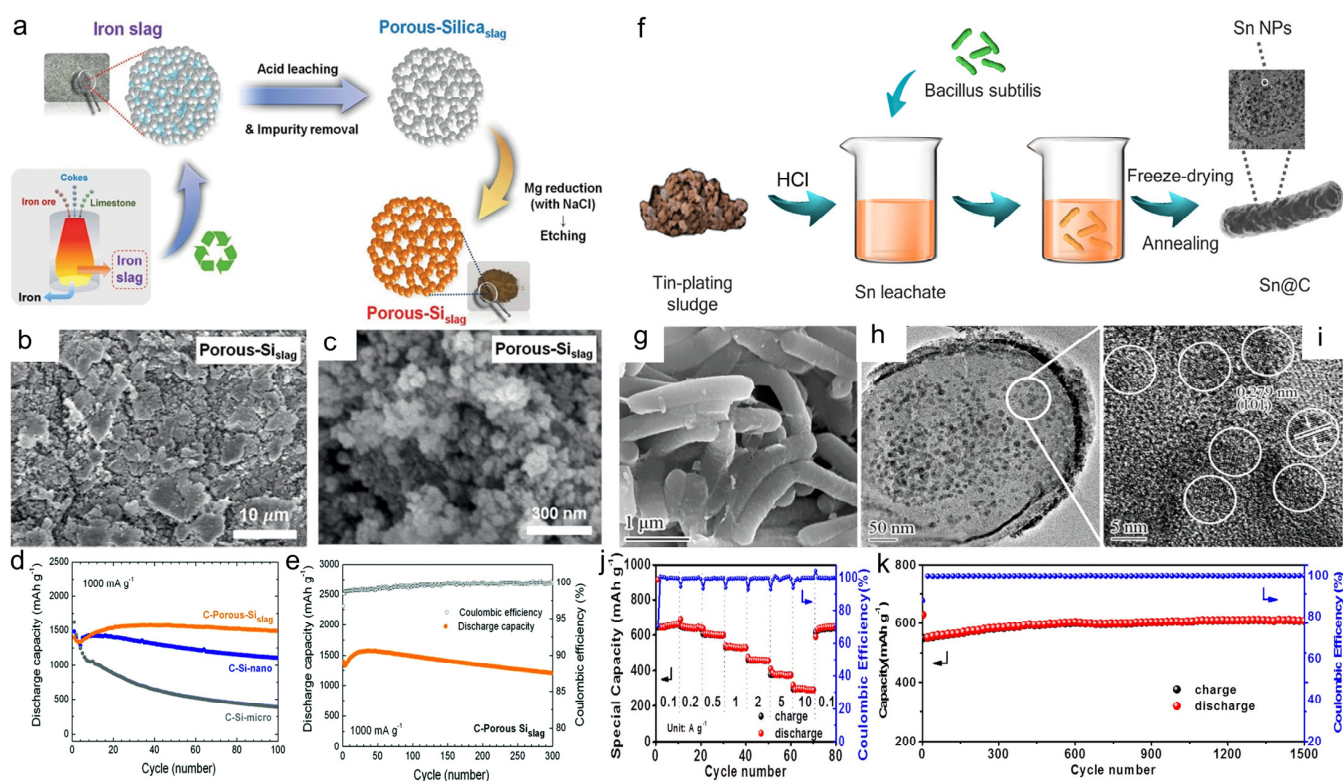


**Figure 1.** (a) Scheme of the synthesis of Porous-Si<sub>slag</sub> from waste iron slag. (b,c) SEM images of Porous-Si<sub>slag</sub>. (d) Cycling properties of C-Si-micro, C-Si-nano, and C-Porous-Si<sub>slag</sub> at 1 A·g<sup>-1</sup>. (e) Long-term cycling performance and CE of C-Porous-Si<sub>slag</sub> at 1 A·g<sup>-1</sup>. Reprinted with permission from ref. [26]. Copyright 2015 Royal Society of Chemistry. (f) Schematic of the fabrication process of Sn@C from tin-plating sludge. (g) SEM image of Sn@C. (h) Transmission electron microscopy (TEM) and (i) high-resolution TEM images of Sn@C. (j) Specific discharge capacity of Sn@C from 0.1 to 10 A·g<sup>-1</sup>. (k) Cyclic performance of Sn@C as the anode of LIB at 1 A·g<sup>-1</sup>. Reprinted with permission from ref. [46]. Copyright 2019 American Chemical Society.

### 2.1.2. Cathode Materials

Cathode materials are an essential part of rechargeable batteries, and cathode materials with high electrochemical performance, low cost, and good working stability are necessary for the development of practical battery systems [50]. The design of cathode materials is closely related to the battery type. For example, LiFePO<sub>4</sub> and LiNi<sub>1-x-y</sub>Co<sub>x</sub>Mn<sub>y</sub>O<sub>2</sub> (NCM) are the most widely studied cathode materials for LIBs, and they have already been commercialized in diverse energy devices [51]. To meet the growing demand of critical metals in LiFePO<sub>4</sub> and NCM, a series of metal-rich mining and metallurgical wastes have been used to fabricate these cathode materials. Steel slag [28], titanium dioxide slag [52], Fe-P waste slag [53], chelate slag [54], vanadium-bearing slag FeSO<sub>4</sub>·7H<sub>2</sub>O [55], waste slag [56,57], extracted vanadium residue [58], and lithium extraction slag [59] are favorable precursors for LiFePO<sub>4</sub>/NCM-based cathode materials. For instance, Yang et al. developed a phosphoric acid mixture selective leaching technique to selectively remove impurity elements (e.g., Mn, Cu, and Ni) from lithium extraction slag, and the recovered FePO<sub>4</sub> (R-FePO<sub>4</sub>) can be directly used as a battery-grade cathode material [59]. Of note, the cost of R-FePO<sub>4</sub> is significantly lower than that of the commercial counterpart (USD 1.35 vs. 2 kg<sup>-1</sup>), indicating the huge economic benefit of reusing waste to construct cathode materials.

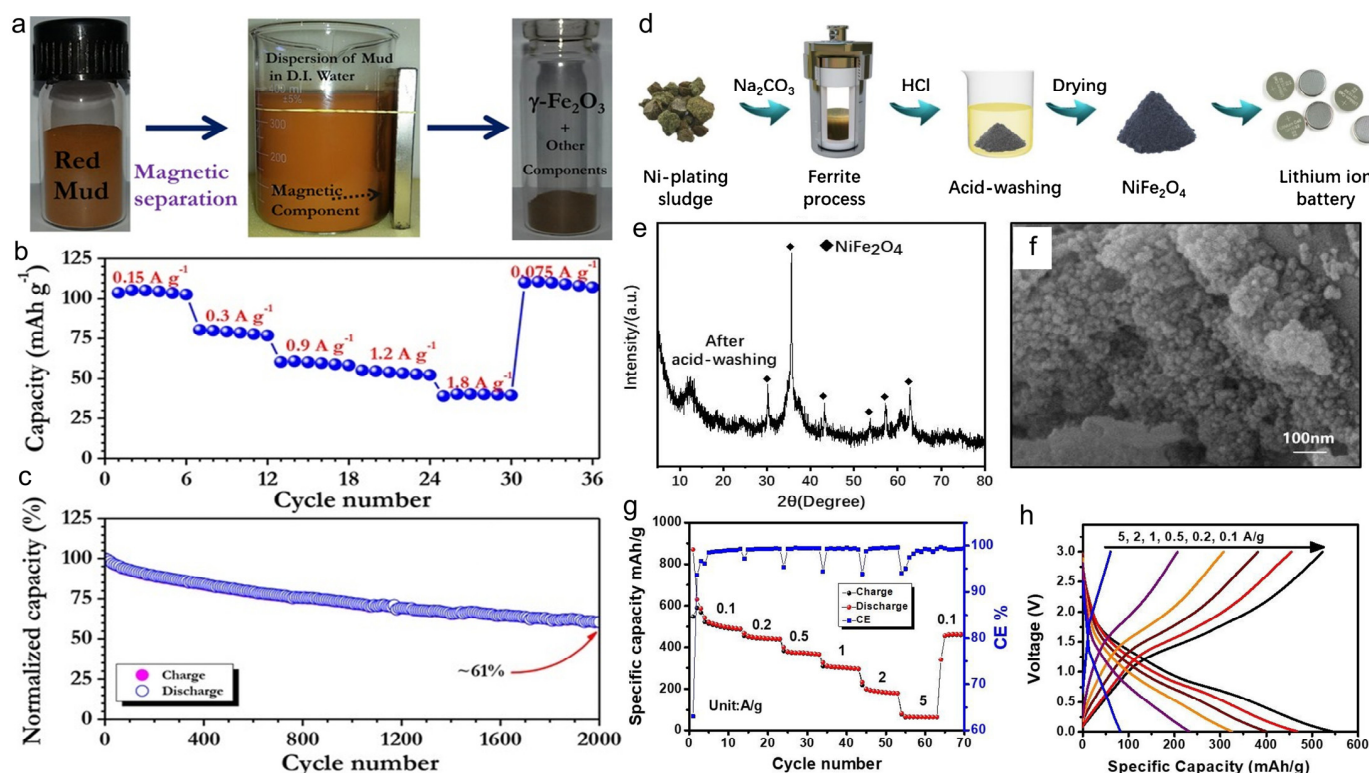


**Figure 2.** (a) Illustration of the extraction of  $\gamma\text{-Fe}_2\text{O}_3$  from red mud. (b) Rate performance of the  $\text{LiMn}_2\text{O}_4/\gamma\text{-Fe}_2\text{O}_3$  full cell and (c) long cycling performance of the  $\text{LiMn}_2\text{O}_4/\gamma\text{-Fe}_2\text{O}_3$  full-cell at 1 A g<sup>-1</sup>. Reprinted with permission from ref. [49]. Copyright 2016 John Wiley and Sons. (d) Scheme of the preparation of  $\text{NiFe}_2\text{O}_4$  nanoparticles from Ni-plating sludge. (e) XRD pattern and (f) SEM image of final products after acid-washing treatment. (g) Specific discharge capacity evolution at different charge/discharge rates. (h) Charge/discharge voltage results of  $\text{NiFe}_2\text{O}_4$  from 0.1 to 5 A g<sup>-1</sup>. Reprinted with permission from ref. [25]. Copyright 2020 Elsevier.

However,  $\text{LiFePO}_4$  and NCM have some disadvantages as cathode materials, such as low conductivity and mediocre activity. To overcome these limitations, waste-derived metal-doped  $\text{LiFePO}_4$  and  $\text{LiFePO}_4/\text{NCM}$ -based composites have gained interest [58]. Starting from  $\text{FeSO}_4 \cdot 7\text{H}_2\text{O}$  waste slag, Wu and coworkers developed a Ti-doped  $\text{LiFePO}_4$  material by a precipitation–ambient temperature reduction method [56]. In the Ti-doped  $\text{LiFePO}_4$ , Ti atoms occupy the Li site, leading to cation-deficient solid solution. The waste-derived Ti-doped  $\text{LiFePO}_4$  cathode can deliver a capacity of 161 mAh g<sup>-1</sup> at 0.1 C and also exhibits high cycling stability at 2 C. Integrating waste-derived  $\text{LiFePO}_4$  with a highly conductive carbon material would significantly improve the performance of cathode materials. Using Fe–P waste slag and glucose as precursors, Kang et al. designed a  $\text{LiFePO}_4/\text{C}$  composite [53]. The  $\text{LiFePO}_4/\text{C}$  with 5.9 wt % carbon has the lowest internal resistance and thus shows improved reaction activity, power capability, and reversibility, as well as decreased polarization degree. Combining the beneficial effects of metal doping and carbon introduction, the preparation of multi-doped  $\text{LiFePO}_4/\text{C}$  from steel slag has been performed [28]. Compared with bare  $\text{LiFePO}_4/\text{C}$ , the presence of Mn, V, and Cr dopants contributes to lower capacity degradation with increasing charge/discharge current density because of improved electrochemical reactivity.

Aside from the LIBs, a group of mining and metallurgical waste-based cathode materials have been successfully applied to AZIBs, Li–S batteries (LSBs), and LOBs. AZIBs with high safety and low cost are emerging energy storage devices, and  $\text{M}_x\text{V}_2\text{O}_5 \cdot n\text{H}_2\text{O}$  ( $\text{M} = \text{Mg}, \text{Ca}, \text{Al}$ , etc.) has attracted growing interest as a cathode material [60,61]. In 2022, Chen and coauthors converted vanadium slag into multi-ion (Fe, Mg, and Ti) pre-intercalated  $\text{V}_2\text{O}_5 \cdot n\text{H}_2\text{O}$  ( $\text{M}_x\text{VO}$ ) via an oxidation–acidification–hydrothermal process (Figure 3a) [29].

The  $M_xVO$  consists of uniform nanoribbons which self-assemble into a micro-flower structure (Figure 3b,c). At  $-20\text{ }^{\circ}\text{C}$ ,  $M_xVO$  attains a specific discharge capacity of  $120\text{ mA h g}^{-1}$  at the high rate of  $50\text{ A g}^{-1}$  (Figure 3d). Typically, the  $M_xVO$  also works well in a practical pouch cell, and Figure 3e suggests that the pouch cell has high rate capability with low polarization at the low temperature of  $-20\text{ }^{\circ}\text{C}$ . LSBs are promising secondary batteries for their large theoretical energy density ( $2600\text{ Wh}\cdot\text{kg}^{-1}$ ) and high theoretical capacity ( $1675\text{ mAh}\cdot\text{g}^{-1}$ ) [62]. Nevertheless, the electrochemical reaction kinetics and shuttle effect of lithium polysulfides (LiPSs) need further improvements, and robust cathode materials are highly required. Using an electroplating sludge precursor, a nano- $\text{Fe}_3\text{C}@\text{N,P}$  co-doped porous carbon ( $\text{Fe}_3\text{C}@\text{NPC}$ ) material has been designed [63]. Benefiting from the main exposed active  $\text{Fe}_3\text{C}$  (220) crystal plane, large SSA, and hierarchically porous spherical structure, the  $\text{Fe}_3\text{C}@\text{NPC}$  cathode material exhibits a high reversible capacity ( $>570\text{ mAh}\cdot\text{g}^{-1}$  at  $1\text{ C}$ , after 500 cycles) and a high reversible CE (over 99%).

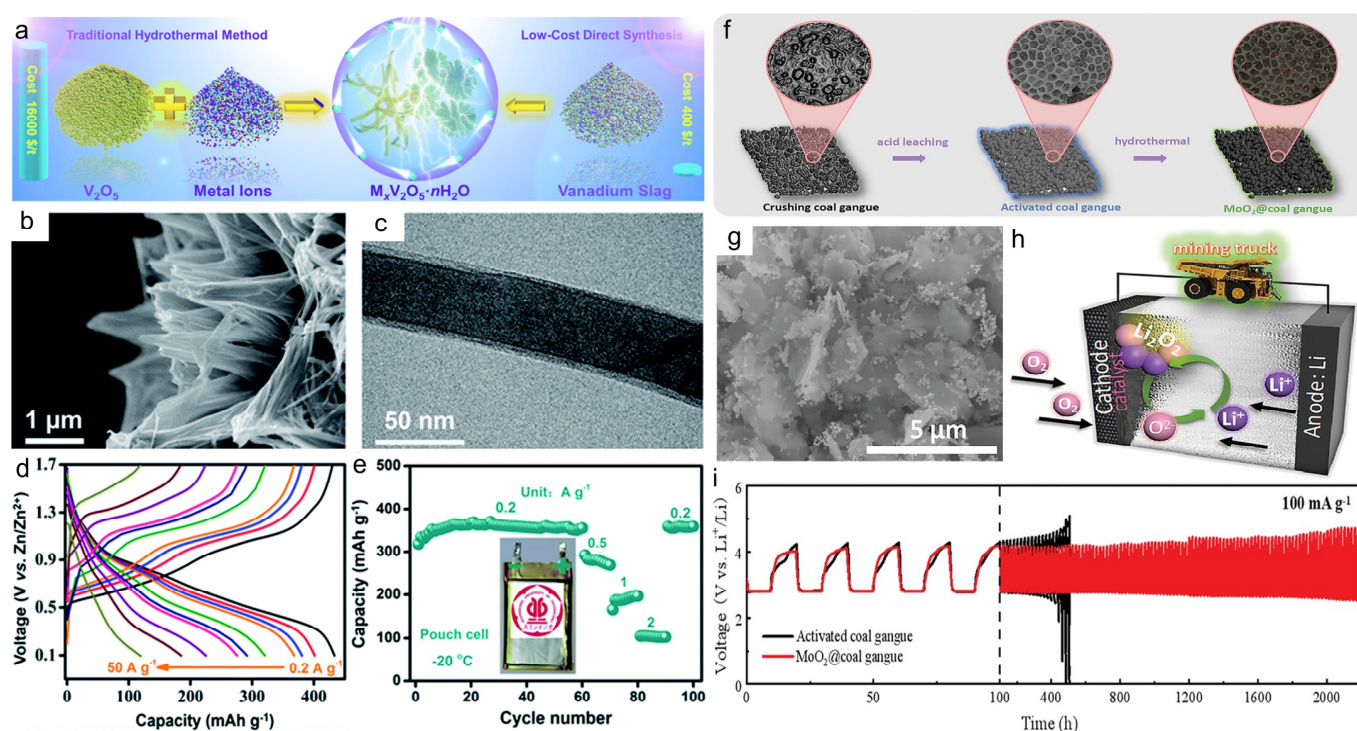


**Figure 3.** (a) Illustration of the synthesis of ion-intercalated  $\text{V}_2\text{O}_5\cdot n\text{H}_2\text{O}$  ( $M_xVO$ ). (b) SEM and (c) TEM images of  $M_xVO$ . (d) Charge/discharge curves of  $M_xVO$  from  $0.2$  to  $50\text{ A}\cdot\text{g}^{-1}$ . (e) Rate performance of flexible Zn/ $M_xVO$  pouch cell. Reprinted with permission from ref. [29]. Copyright 2022 Royal Society of Chemistry. (f) Scheme of the fabrication of  $\text{MoO}_2@\text{coal gangue}$ . (g) SEM image of  $\text{MoO}_2@\text{coal gangue}$ . (h) Scheme of LOBs. (i) Discharge/charge cycling profiles of  $\text{MoO}_2@\text{coal gangue}$ -based LOBs at  $100\text{ mA g}^{-1}$  (cut-off capacity:  $1000\text{ mAh}\cdot\text{g}^{-1}$ ). Reprinted with permission from ref. [27]. Copyright 2023 John Wiley and Sons.

LOBs attract great scientific interest for their ultrahigh theoretical energy density ( $3500\text{ Wh}\cdot\text{kg}^{-1}$ ) [64]. The main performance limitation of LOBs is the sluggish electrode reaction kinetics, namely, the oxygen evolution/reduction at the cathode. Starting from coal gangue, Sun and coauthors developed an acid–alkali activation process to fabricate an amorphous  $\text{SiC}_x/\text{SiO}_x$  catalyst with abundant functional groups and rich oxygen vacancies [65]. The  $\text{SiC}_x/\text{SiO}_x$  catalyst involved LOBs and has a high discharge capacity ( $9156\text{ mAh}\cdot\text{g}^{-1}$ ) and boosted cycling stability ( $>350\text{ h}$ ). However, the oxygen evolution/reduction performance of the  $\text{SiC}_x/\text{SiO}_x$  catalyst is unclear. For another coal gangue-derived  $\text{MoO}_2@\text{coal gangue}$  electrocatalyst prepared by an acid leaching–hydrothermal process (Figure 3f,g) [27], density functional theory (DFT) calculations suggest that the unique amorphous/crystalline

structure, the synergistic effect between stable  $\text{SiO}_2$  and highly active  $\text{MoO}_2$ , and the regulated  $\text{LiO}_2$  intermediate adsorption altogether contribute to the high performance (a high initial discharge capacity of  $9748 \text{ mAh}\cdot\text{g}^{-1}$  with a long-term cycling stability  $> 2200 \text{ h}$ ; Figure 3h,i).

The wide applications of mining and metallurgical waste-derived metal oxides, silicon (oxides), and related composites in rechargeable batteries well demonstrate the feasibility of developing waste-based electrodes for next-generation low-cost battery systems. The elaborate control of chemical composition, size, and nanostructure helps to develop high-performance waste-derived electrode materials, and many of the waste-derived materials show comparable performances to those prepared from commercial chemicals.

## 2.2. Supercapacitors

Supercapacitors are widely used as portable power storage devices because of their high power density and fast charge/discharge process, as well as good cycling stability [66,67]. Low-cost metal-based materials exhibit high charge storage capacities governed by electrical double-layer capacitance and/or pseudocapacitance. Recently, many metal-rich mining and metallurgical waste-derived metal (hydr)oxides and composite materials have been investigated for the supercapacitor application.

### 2.2.1. Metal (Hydr)oxide Materials

The capacitance of metal (hydr)oxides is significantly related to their theoretical-specific capacitance and nanostructure. Fe/Ni/Co-based (hydr)oxides with high intrinsic redox activities are widely studied in electrochemistry [68]. These metal elements are also rich in different mining and metallurgical wastes, giving the opportunity to develop high-performance electrodes from waste. Chen et al. designed an  $\text{Fe}_2\text{O}_3$  material from vanadium titanomagnetite tailings with the Fe-based metal-organic framework (MOF) as a reaction intermediate (Figure 4a) [19]. Derived from the MOF precursor, the as-prepared  $\text{Fe}_2\text{O}_3$  material has a small particle size and loose porous structure, which contributes to large SSA and finally benefits the electrolyte/charge transfer. The assembled NiCo(O)S// $\text{Fe}_2\text{O}_3$  asymmetric supercapacitor outperforms a series of  $\text{Fe}_2\text{O}_3$ -based supercapacitors and can preserve 80.2% capacitance after 7000 cycles at  $5 \text{ A}\cdot\text{g}^{-1}$  (Figure 4b,c). Red mud [69] and ground-granulated blast furnace slag [70] also show high potential as precursors of  $\text{Fe}_2\text{O}_3$  to construct supercapacitors. Nickel bicarbonate is another widely used electrode for supercapacitors. Hou and coworkers have designed amorphous hollow  $\text{Ni}(\text{HCO}_3)_2$  from Ni-containing electroplating sludge via a hydrothermal method [12]. Interestingly, the  $\text{Ni}(\text{HCO}_3)_2$  spheres self-assemble into a hollow sphere structure, and the surface of the integrated sphere possesses abundant nanowires. The as-formed structure benefits the full contact of electrolyte and electrode, and further accelerates the electrochemical reactions. The optimal sample with ascorbic acid (AA) as the complexing agent shows a better activity than its analogues, and it can provide a high rate capability of 61.02% at  $10 \text{ A}\cdot\text{g}^{-1}$  and a good cycling performance (52.09% capacitance retention after 1000 cycles).

Transition metal-based layered double hydroxides (LDHs) synthesized from electroplating sludge have been used for supercapacitors [31,71]. The  $\beta\text{-Ni}(\text{OH})_2$  powder prepared from a spent electroless nickel plating bath has a high specific capacitance of  $332 \text{ F}\cdot\text{g}^{-1}$  at  $5 \text{ mV}\cdot\text{s}^{-1}$ , mainly due to the pseudocapacitance property of  $\beta\text{-Ni}(\text{OH})_2$  [31]. For the NiFeAl LDHs hydrothermally synthesized from electroplating sludge, the utilization of urea in the synthesis process leads to decreased particle size and large SSA [71]. In addition, the presence of the urea-derived  $-\text{O}-\text{C}\equiv\text{N}$  group on the NiFeAl LDH surface promotes electron transfer efficiency and further improves the high supercapacitor performance (specific capacitance of  $1652.20 \text{ F}\cdot\text{g}^{-1}$  at  $0.5 \text{ A}\cdot\text{g}^{-1}$ , and 46.4% capacitance preserved after 1000 cycles). In this study, the performance is centrally ascribed to active Ni by the authors, while the role of Fe and Al in the LDHs is unclear.

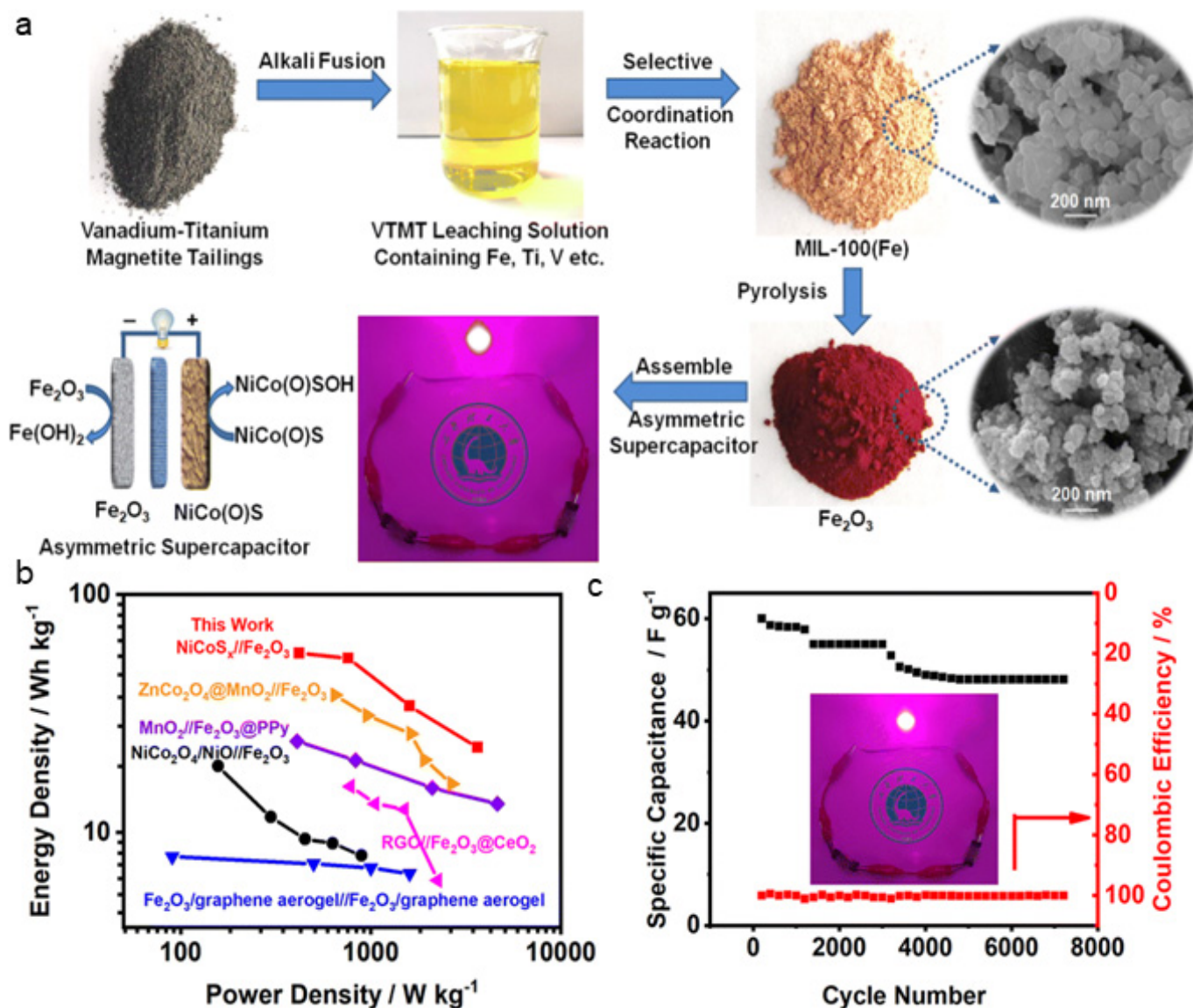


**Figure 4.** (a) Scheme of synthesis of Fe<sub>2</sub>O<sub>3</sub> from vanadium titanomagnetite tailings and its utilization in asymmetric supercapacitors. (b) Ragone plot of NiCo(O)S//Fe<sub>2</sub>O<sub>3</sub> asymmetric supercapacitor and its counterparts. (c) Long-term cycling profile of NiCo(O)S//Fe<sub>2</sub>O<sub>3</sub> asymmetric supercapacitor. Reprinted with permission from ref. [19]. Copyright 2023 Royal Society of Chemistry.

## 2.2.2. Composite Materials

Aiming at improving the conductivity and activity of metal (hydr)oxides, some mining and metallurgical waste-derived composite materials have been developed [72,73]. Integrating highly conductive carbon materials (e.g., graphene (oxide) [74–76] and biomass carbon [30]) with waste-derived metal materials is extensively studied to construct high-performance electrode materials [77]. For example, Muthukannan et al. prepared an Fe<sub>3</sub>O<sub>4</sub>/rGO composite via a hydrothermal process from iron ore tailings [74]. With enhanced interfacial conductivity and augmented resourceful surface area, the composite outperforms the corresponding single-component electrode materials.

Alternatively, the combination of two electroactive materials is another way to construct efficient electrode materials for supercapacitors [78]. For instance, Hou and coauthors converted nickel-containing electroplating sludge into an Fe, Al dual-doped  $\alpha$ -Ni(OH)<sub>2</sub>/Ni(HCO<sub>3</sub>)<sub>2</sub> composite for pseudocapacitors [79]. This composite makes full use of different metal elements (Ni, Fe, and Al) in the electroplating sludge. Interestingly,

Al and Fe dopants increase the interlayer distance of  $\alpha$ -Ni(OH)<sub>2</sub> and thus promote the diffusion of OH<sup>−</sup> and enhance the electrochemical activity of the composite. Additionally, the  $\alpha$ -Ni(OH)<sub>2</sub>/Ni(HCO<sub>3</sub>)<sub>2</sub> composite with a hierarchical structure offers abundant electroactive sites for the OH<sup>−</sup> in the electrolyte and full contact of reactants. Benefiting from these advantages, the  $\alpha$ -Ni(OH)<sub>2</sub>/Ni(HCO<sub>3</sub>)<sub>2</sub> composite-based asymmetric supercapacitor attains a large energy density of over 30 Wh·kg<sup>−1</sup> at 0.37 kW·kg<sup>−1</sup>.

As important energy storage devices, supercapacitors hold the promise of efficient portable power storage. The development of mining and metallurgical waste-derived electroactive materials largely cuts the fabrication cost of supercapacitors. With rich transition metals, mining and metallurgical waste can be used to develop materials (e.g., metal (hydr)oxides and their composites) with high electrical double-layer capacitance and pseudocapacitance. Waste-derived nanostructured electroactive materials with high SSAs are favorable for the supercapacitor application.

### 2.3. Fuel Cells

Fuel cells are promising eco-friendly devices to convert chemical energy of fuels into electrical energy, which have been commercialized to supply energy to stationary and portable facilities [80–82]. Depending on the property of fuels (e.g., carbon, H<sub>2</sub>, and methanol) and electrolytes (e.g., polymer electrolytes, solid oxides, molten salts, and alkalis), diverse fuel cell systems have been developed. In fuel cells, electroactive materials are important for the system efficiency and capacity. To date, a group of mining and metallurgical waste-derived electroactive materials have been fabricated for applications in DC-SOFCs [83], direct methanol fuel cells (DMFCs) [84], and MFCs [85].

DC-SOFCs can directly convert solid carbon's chemical energy into electricity via the electrooxidation reaction [86]. In the anode chamber, the efficiency of the reverse Boudouard reaction largely governs the performance of DC-SOFCs. As such, designing cost-effective catalysts for the Boudouard reaction is highly urgent. Recently, strontium slag [32,83] and steel slag [87] have been used for constructing Boudouard reaction catalysts. In Han et al.'s study, the application of strontium slag-derived catalysts can improve the DC-SOFC output from 189 to 248 mW·cm<sup>−2</sup> at 850 °C, and the improved system attains a fuel utilization of 25.6% [83]. However, it is quite challenging to figure out the catalytic mechanism and the catalytically active site because the strontium slag-derived catalyst is a mixture of SrCO<sub>3</sub>, CaCO<sub>3</sub>, Fe<sub>2</sub>O<sub>3</sub>, MgO, and Al<sub>2</sub>O<sub>3</sub>. For the steel slag-derived catalyst, Jiao et al. proposed that the main active components were oxides of calcium and iron [87], but no solid evidence has been provided. To improve the performance of DMFCs, red mud has been used to modify chitosan–polyvinyl alcohol (PVA) membranes [84]. Note that red mud enhances the ion exchange capacity, thermal stability, and bound water content of the composite membrane. The three-component membrane can provide a maximum power density of 44 mW·cm<sup>−2</sup> at 140 mA·cm<sup>−2</sup>.

MFCs are important bioelectrochemical devices for simultaneous energy generation and wastewater treatment [88]. The power output of MFCs is largely affected by the electron transfer efficiency, which can be regulated by applying anode materials. Jadhav et al. found that the application of heat-treated goethite (recovered from mining mud) as the anode active material could lead to a fivefold increment in power, compared with the bare stainless-steel anode (17.1 vs. 3.5 W·m<sup>−3</sup>) [20]. The main reason is that the presence of goethite promotes the electron transfer efficiency between bacteria and the anode. In another sediment microbial fuel cell (SMFC), the application of steel slag also increases the generated power through decreasing the concentration loss during the electron transfer process from bacteria to anode [85].

Currently, only several studies have focused on mining and metallurgical waste-derived electroactive materials for fuel cell applications. Most of these waste-derived materials show a complex composition of metal oxides, and more studies are suggested to figure out the contributions of different components to electrochemical performance with quantitative and advanced analytical techniques.

## 2.4. Small-Molecule Conversion

Recently, the electrochemical conversion of small molecules (e.g., CO<sub>2</sub>, H<sub>2</sub>O, O<sub>2</sub>, and N<sub>2</sub>) has aroused great research interest due to their critical role in energy conversion and energy-related carbon neutrality processes [89–93]. Electrocatalysts are critical for the conversion of small molecules, which can tune the reaction selectivity, reduce the reaction energy barrier, and accelerate the reaction kinetics [94,95]. In this context, catalysts with high activity, good stability, and low cost are highly needed. Hitherto, some catalysts developed from mining and metallurgical waste show promising performance towards CO<sub>2</sub> reduction, N<sub>2</sub>/nitrate reduction, and water oxidation, which are detailed in this section.

### 2.4.1. Materials for CO<sub>2</sub> Reduction

Electrochemical reduction of CO<sub>2</sub> to value-added fuels and chemicals is an important route to utilize the excess greenhouse gases. The reduction products are highly catalyst-dependent, and Sn, Cu, Ag-based catalysts are extensively studied. Zhong et al. developed a Sn@NPC catalyst (Sn nanoparticles loaded on N, P co-doped carbon) from Sn electroplating sludge [22]. The Sn@NPC catalyst exhibits a high FE (87.93%) for HCOOH at 1.05 V vs. RHE. DFT calculations suggest that Sn@NPC can improve the adsorption of CO<sub>2</sub>/<sup>\*</sup>OCHO and the desorption of <sup>\*</sup>HCOOH, leading to promoted performance. Using fayalite slags as the metal precursor, Yang and coauthors designed a series of copper–lead catalysts with varying Cu/Pb ratios for CO<sub>2</sub> reduction (Figure 5a) [33]. It is interesting to find a volcano-shape relationship between product selectivity toward CO and HCOOH and the Cu/Pb ratio of catalysts (Figure 5b,c). To attain a high FE for the CO product, Cu<sub>9.00</sub>Pb<sub>1.00</sub> is preferred. Further in situ analysis suggests that the optimized Pb amount can effectively improve the reducibility of Pb<sup>2+</sup> and Cu<sup>1+</sup> species in pristine catalysts to metallic Pb and Cu (Figure 5d), thereby boosting the CO selectivity by synergistic effects of Pb<sup>0</sup> and Cu<sup>0</sup>.

CO<sub>2</sub> reduction in microbial electrolysis cells (MECs) has also been investigated. In MECs, potential can be generated at bioanodes by organic substrates, and less power is needed for cathodic CO<sub>2</sub> reduction than in conventional electrolytic cells [96]. Yuan et al. developed a pyrolysis process to convert electroplating sludge into an active catalyst for CO<sub>2</sub> reduction in a MEC [97]. The sludge-derived catalyst can promote the CO<sub>2</sub>-to-methane conversion with a production rate of ~42 mmol·h<sup>−1</sup>·m<sup>−2</sup>. However, the multiple phases (e.g., FeNi, CuNi, CuFeS, NiO, Cu<sub>2</sub>O, and Ni(OH)<sub>2</sub>) in the catalyst make it quite difficult to investigate the CO<sub>2</sub> reduction mechanism on an atomic scale.

### 2.4.2. Materials for N<sub>2</sub>/Nitrate Reduction

Electrocatalytic N<sub>2</sub>/nitrate-to-ammonia conversion has become a promising process to produce green ammonia, which is a high-density energy carrier. To obtain a high ammonia yield and selectivity at lower cost, efforts have been made to design electrocatalysts from mining and metallurgical waste. With a Cu, Cr-containing electroplating sludge precursor, Zhang et al. designed CuCr<sub>2</sub>O<sub>4</sub>-dominated phase catalysts for N<sub>2</sub> reduction [34]. Under ambient conditions, the electroplating sludge-derived catalyst shows a higher ammonia yield than the counterpart synthesized from pure reagents (15.9 vs. 9.8 μg·h<sup>−1</sup>·mg<sup>−1</sup><sub>cat</sub>). The reason should be the high amounts of Fe, Mg dopants, as well as the rich oxygen vacancy in the sludge-derived catalyst. In another study, four electroplating sludge samples have been used to synthesize ZnCr<sub>2</sub>O<sub>4</sub>, CuCr<sub>2</sub>O<sub>4</sub>, and NiCr<sub>2</sub>O<sub>4</sub> catalysts for N<sub>2</sub> reduction [98]. Among the three catalysts, CuCr<sub>2</sub>O<sub>4</sub> shows a higher NH<sub>3</sub> yield of 8.86 μg·h<sup>−1</sup>·mg<sup>−1</sup><sub>cat</sub> (−0.9 V vs. RHE), with an FE of 0.57%. The authors also pointed out the beneficial role of metal dopants and oxygen vacancy in the N<sub>2</sub> adsorption and reduction processes.

Compared with N<sub>2</sub> reduction, nitrate-to-ammonia conversion is easier because the breaking of polar N–O bonds is more feasible than the splitting of inert N≡N [99]. Recently, Xu et al. directly used red mud for nitrate reduction [35]. The red mud catalyst has a complex phase property, and Fe<sub>2</sub>O<sub>3</sub>, AlO(OH), CaCO<sub>3</sub>, katoite, and cancrinite can be identified. The authors suggested that Fe<sub>2</sub>O<sub>3</sub> (mass ratio of 29.2%) is the active phase for nitrate reduction. At −0.73 V vs. RHE, the catalyst shows a high NH<sub>3</sub> generation rate of

$160 \mu\text{mol cm}^{-2}\cdot\text{h}^{-1}$  and a high FE of 92.8%. When further integrated with a photovoltaic system, the solar-to-ammonia conversion efficiency reaches 2.09%. This study demonstrates the high potential of mining and metallurgical wastes as efficient catalysts for zero-carbon ammonia-energy generation.

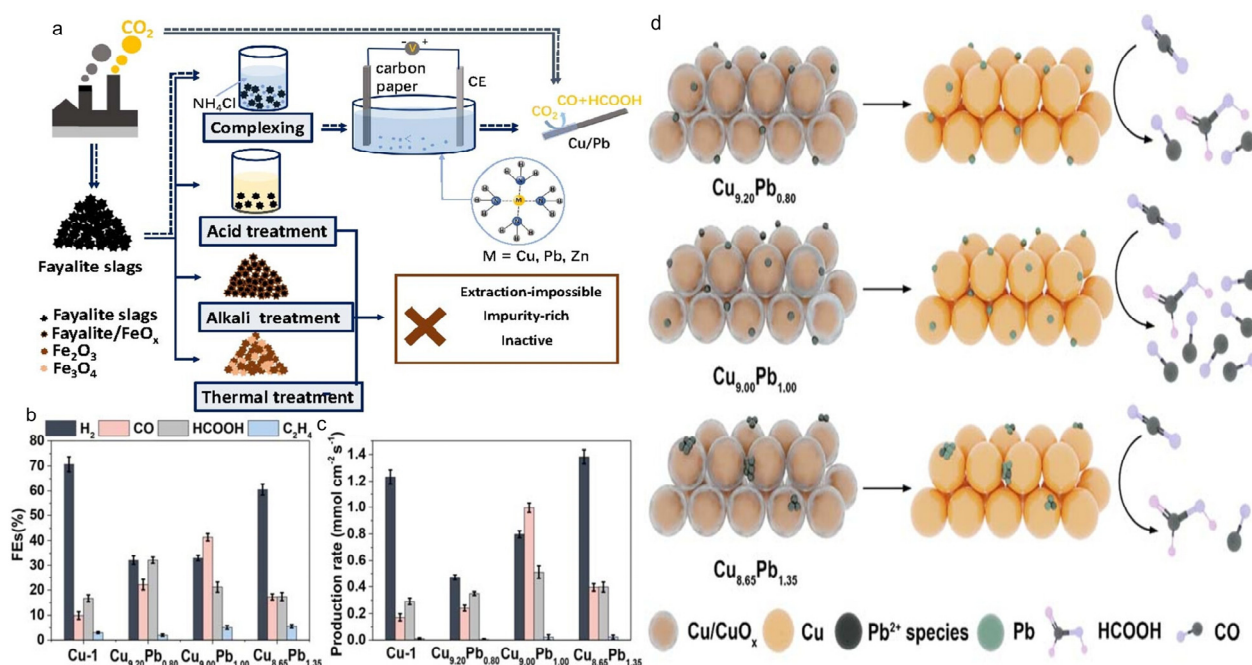


**Figure 5.** (a) Illustration of fabrication of Cu-Pb catalysts from fayalite slags. (b) FE and (c) production rates of main products for Cu-Pb catalysts at  $-1.05 \text{ V}$  vs. RHE. (d) Scheme of the in situ reconstruction of Cu-Pb catalysts during CO<sub>2</sub> reduction. Reprinted with permission from ref. [33]. Copyright 2022 John Wiley and Sons.

#### 2.4.3. Materials for Water Oxidation

Hydrogen energy is important for the sustainable development of clean energy systems [100–102]. Water electrolysis is an efficient route to produce high-purity hydrogen fuel in a sustainable and green manner [103–105]. Compared with the two-electron hydrogen evolution reaction (HER) at the cathode part, the four-electron OER is more energy-demanding and limits the water electrolysis efficiency [106–109]. As such, developing high-performance OER catalysts is an urgent mission. Recently, some studies have constructed catalysts from hydrometallurgical wastewater [21,110]. Chen et al. developed a boriding method to convert multiple metal ions in hydrometallurgical wastewater into a series of FeNiCuSnB (FNCSB) catalysts with different element ratios (Figure 6a) [21]. The as-prepared FNCSB catalyst shows a coral-like interconnected nanostructure, with rich pores (Figure 6b,c). Compared with the commercial RuO<sub>2</sub> catalyst, FNCSB catalysts exhibit better performance towards OER, in terms of  $\eta_{10}$  and Tafel slope (Figure 6d,e). In particular, the composition-optimized FNCSB-4 (Fe<sub>4.8</sub>Ni<sub>36.4</sub>Cu<sub>0.9</sub>Sn<sub>1.3</sub>B<sub>28.1</sub>O<sub>28.5</sub>) has a low  $\eta_{10}$  of 199 mV and a Tafel slope of 53.98 mV dec<sup>-1</sup>, outperforming a group of transition metal-based catalysts (Figure 6f). The same research group also developed an electrodeposition–electrolysis technique to develop bifunctional NiCoMn layered triple hydroxide electrocatalysts for hydrogen production from wastewater [111].

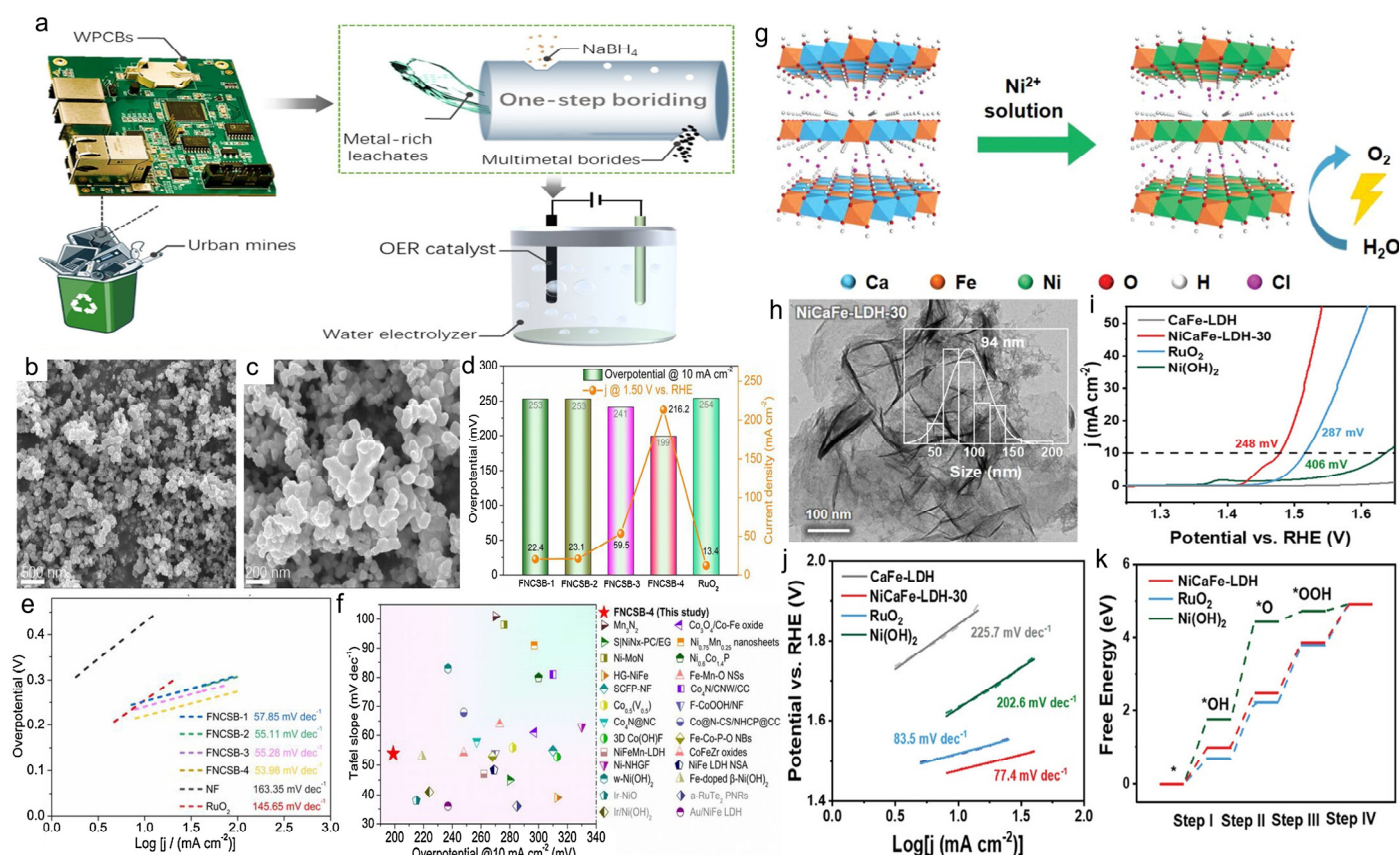


**Figure 6.** (a) Scheme of the boriding conversion process. (b,c) SEM images of FNCSB-4. (d) Current densities at 1.50 V vs. RHE and  $\eta_{10}$ , and (e) corresponding Tafel plots of FNCSBs and the RuO<sub>2</sub> catalyst. (f) Comparison of OER performance of FNCSB-4 and a group of transitional metal-based catalysts. Reprinted with permission from ref. [21]. Copyright 2021 Elsevier. (g) Illustration of the conversion of Ni<sup>2+</sup> to NiCaFe-LDH catalyst. (h) TEM image of NiCaFe-LDH-30. (i) Linear sweep voltammetry curves and (j) corresponding Tafel plots of catalysts. (k) DFT calculations of OER free energy profiles of Ni(OH)<sub>2</sub>, RuO<sub>2</sub>, and NiCaFe-LDH. Reprinted with permission from ref. [112]. Copyright 2022 John Wiley and Sons.

To make use of Ni<sup>2+</sup> in electroplating wastewater, Chi et al. used CaFe-LDH as a mineralizer to develop a NiCaFe-LDH catalyst (Figure 6g) [112]. The optimal NiCaFe-LDH-30 catalyst has a nanosheet structure, with a mean size of 94 nm (Figure 6h). Electrochemical tests suggest that NiCaFe-LDH-30 possesses better OER performance ( $\eta_{10}$  = 248 mV, Tafel slope = 77 mV dec<sup>-1</sup>) than Ni(OH)<sub>2</sub> and CaFe-LDH, as well as the RuO<sub>2</sub> catalyst (Figure 6i,j). The high activities of NiCaFe-LDH are further explained by DFT calculations (Figure 6k). The OER potential-determining step (PDS) of NiCaFe-LDH is the Step II with an energy barrier ( $\Delta G_{II}$ ) of 1.50 eV, which is lower than that of Ni(OH)<sub>2</sub> (PDS: Step II,  $\Delta G_{II}$  = 2.69 eV) and RuO<sub>2</sub> (PDS: Step III,  $\Delta G_{III}$  = 1.56 eV).

Electrochemistry-driven small-molecule conversion is critical for the decarbonization of global energy systems, and the development of cost-effective catalysts is urgent. Current efforts in converting mining and metallurgical waste into nanostructured electrocatalysts (e.g., metal oxides, hydroxides, alloys, borides, and related composites) would largely sustain the development of related electrochemical energy conversion processes. As electrocatalytic performance is sensitive to the surface morphology and electronic properties of catalysts, many studies have emphasized composition regulation and nanostructure control to obtain high-performance waste-derived catalysts.

### 3. Conclusions and Perspectives

In this review, the recent achievements in the application of mining and metallurgical waste-derived electroactive materials for advanced energy systems (batteries, supercapacitors, fuel cells, and small-molecule conversion) are comprehensively analyzed. The waste-to-electroactive materials conversion methods, performance, and structure–performance relationships are well illustrated. In some cases, the waste-derived electroactive materials outperform those synthesized from stored chemicals, suggesting the high potential of developing waste-based cost-effective materials. Nevertheless, there are some central challenges that need further exploration.

First, it is important to identify the origin of the electrochemical activity of mining and metallurgical waste-derived materials, since most mining and metallurgical waste has a complex composition, with diverse impurities. This feature makes it difficult to investigate the active sites that are involved in electrochemical reactions. Thus, one should carefully check the chemical composition and phase structure of waste-derived materials with advanced techniques (e.g., inductively coupled plasma spectroscopy, TEM, and XRD), which can provide useful information for the analysis of physicochemical property–performance relationships.

Second, it is feasible to co-transform mining and metallurgical waste and biowaste for constructing high-performance carbon-based composite materials, as a main group of mining and metallurgical waste-derived materials are in the form of metal (hydr)oxides which have a disadvantage of low conductivity. Via integrating biowaste-derived conductive carbon, it is foreseeable that low-cost carbon-based hybrids would outperform the single metal (hydr)oxide counterparts. In addition, biowaste-to-carbon material conversion also can help to tackle biowaste-related pollution issues.

Third, mining and metallurgical waste-derived materials can be applied in large-scale industrial applications. Current studies have verified the feasibility of using mining and metallurgical waste-derived materials in diverse energy systems on a lab scale. To meet the requirements of industrial applications, it is necessary to develop efficient methods to realize the large-scale preparation of electroactive materials from mining and metallurgical waste. Also, testing the activity and stability of these waste-derived materials in industrial energy devices is crucial for their further applications.

**Author Contributions:** F.G.: writing—original draft preparation; Q.C.: writing—review and editing; Z.L.: writing—review and editing; D.C.: writing—review and editing; N.H.: writing—review and editing; Z.C.: conceptualization, writing—review and editing, supervision. All authors have read and agreed to the published version of the manuscript.

**Funding:** This research received no external funding.

**Data Availability Statement:** This article does not provide new data.

**Conflicts of Interest:** The authors declare no conflict of interest.

### References

1. Xavier, L.H.; Ottoni, M.; Abreu, L.P.P. A comprehensive review of urban mining and the value recovery from e-waste materials. *Resour. Conserv. Recycl.* **2023**, *190*, 106840. [[CrossRef](#)]
2. Šajn, R.; Ristović, I.; Čeplak, B. Mining and Metallurgical Waste as Potential Secondary Sources of Metals—A Case Study for the West Balkan Region. *Minerals* **2022**, *12*, 547. [[CrossRef](#)]
3. Chen, Z.; Ren, Z.; Zheng, R.; Gao, H.; Ni, B.-J. Migration behavior of impurities during the purification of waste graphite powders. *J. Environ. Manag.* **2022**, *315*, 115150. [[CrossRef](#)] [[PubMed](#)]
4. Makhathini, T.P.; Bwapwa, J.K.; Mtsweni, S. Various Options for Mining and Metallurgical Waste in the Circular Economy: A Review. *Sustainability* **2023**, *15*, 2518. [[CrossRef](#)]
5. Araujo, F.S.M.; Taborda-Llano, I.; Nunes, E.B.; Santos, R.M. Recycling and Reuse of Mine Tailings: A Review of Advancements and Their Implications. *Geosciences* **2022**, *12*, 319. [[CrossRef](#)]
6. Kaniki, A.T.; Tumba, K. Management of mineral processing tailings and metallurgical slags of the Congolese copperbelt: Environmental stakes and perspectives. *J. Clean. Prod.* **2019**, *210*, 1406–1413. [[CrossRef](#)]

7. Chen, Z.; Yun, S.; Wu, L.; Zhang, J.; Shi, X.; Wei, W.; Liu, Y.; Zheng, R.; Han, N.; Ni, B.-J. Waste-Derived Catalysts for Water Electrolysis: Circular Economy-Driven Sustainable Green Hydrogen Energy. *Nano-Micro Lett.* **2023**, *15*, 4. [\[CrossRef\]](#)
8. Yang, T.; Niu, Y.; Liu, Q.; Xu, M. Cathode host engineering for non-lithium (Na, K and Mg) sulfur/selenium batteries: A state-of-the-art review. *Nano Mater. Sci.* **2023**, *5*, 119–140. [\[CrossRef\]](#)
9. Chen, Z.; Zheng, R.; Graš, M.; Wei, W.; Lota, G.; Chen, H.; Ni, B.-J. Tuning electronic property and surface reconstruction of amorphous iron borides via W-P co-doping for highly efficient oxygen evolution. *Appl. Catal. B Environ.* **2021**, *288*, 120037. [\[CrossRef\]](#)
10. Zhang, Y.; Fu, C.; Weng, S.; Lv, H.; Li, P.; Deng, S.; Hao, W. Construction of an “environment-friendly” CuBx@PU self-supporting electrode toward efficient seawater electrolysis. *Green Chem.* **2022**, *24*, 5918–5929. [\[CrossRef\]](#)
11. Pei, Y.R.; Zhao, M.; Zhu, Y.P.; Yang, C.C.; Jiang, Q. VN nanoparticle-assembled hollow microspheres/N-doped carbon nanofibers: An anode material for superior potassium storage. *Nano Mater. Sci.* **2022**, *4*, 104–112. [\[CrossRef\]](#)
12. Hou, Z.; Meng, H.; Shao, X.; Wang, X.; Tahir, M.U.; Ahmad, S.; Yang, C.; Su, X.; Zhang, L. Synthesis of amorphous hollow Ni(HCO<sub>3</sub>)<sub>2</sub> nanostructures with excellent supercapacitor performance from nickel-containing electroplating sludge. *J. Environ. Chem. Eng.* **2022**, *10*, 106906. [\[CrossRef\]](#)
13. Zhang, K.; Cen, Z.; Yang, F.; Xu, K. Rational construction of NiCo<sub>2</sub>O<sub>4</sub>@Fe<sub>2</sub>O<sub>3</sub> core-shell nanowire arrays for high-performance supercapacitors. *Prog. Nat. Sci. Mater. Int.* **2021**, *31*, 19–24. [\[CrossRef\]](#)
14. Yao, J.; Li, H.; Li, Y.; Yang, J.; Liu, B. Based on the utilization of jarosite residue: The lithium storage performance of α-Fe<sub>2</sub>O<sub>3</sub> materials synthesized from different iron solution systems. *J. Electroanal. Chem.* **2022**, *907*, 116085. [\[CrossRef\]](#)
15. Oh, K.-S.; Lee, J.E.; Lee, Y.-H.; Jeong, Y.-S.; Kristanto, I.; Min, H.-S.; Kim, S.-M.; Hong, Y.J.; Kwak, S.K.; Lee, S.-Y. Elucidating Ion Transport Phenomena in Sulfide/Polymer Composite Electrolytes for Practical Solid-State Batteries. *Nano-Micro Lett.* **2023**, *15*, 179. [\[CrossRef\]](#)
16. Chen, Z.; Duan, X.; Wei, W.; Wang, S.; Ni, B.-J. Recent advances in transition metal-based electrocatalysts for alkaline hydrogen evolution. *J. Mater. Chem. A* **2019**, *7*, 14971–15005. [\[CrossRef\]](#)
17. Yu, K.; Yang, H.; Zhang, H.; Huang, H.; Wang, Z.; Kang, Z.; Liu, Y.; Menezes, P.W.; Chen, Z. Immobilization of Oxyanions on the Reconstructed Heterostructure Evolved from a Bimetallic Oxy-sulfide for the Promotion of Oxygen Evolution Reaction. *Nano-Micro Lett.* **2023**, *15*, 186. [\[CrossRef\]](#)
18. Yao, J.; Yang, Y.; Li, Y.; Jiang, J.; Xiao, S.; Yang, J. Interconnected α-Fe<sub>2</sub>O<sub>3</sub> nanoparticles prepared from leaching liquor of tin ore tailings as anode materials for lithium-ion batteries. *J. Alloys Compd.* **2021**, *855*, 157288. [\[CrossRef\]](#)
19. Chen, J.; Qian, L.; Fu, Z.; Li, G.; Zeng, Y. Recycling of iron from vanadium titanium magnetite tailings and its application in an asymmetric supercapacitor. *New J. Chem.* **2023**, *47*, 9383–9391. [\[CrossRef\]](#)
20. Jadhav, D.A.; Ghadge, A.N.; Ghangrekar, M.M. Enhancing the power generation in microbial fuel cells with effective utilization of goethite recovered from mining mud as anodic catalyst. *Bioresour. Technol.* **2015**, *191*, 110–116. [\[CrossRef\]](#)
21. Chen, Z.; Zheng, R.; Zou, W.; Wei, W.; Li, J.; Wei, W.; Ni, B.-J.; Chen, H. Integrating high-efficiency oxygen evolution catalysts featuring accelerated surface reconstruction from waste printed circuit boards via a boriding recycling strategy. *Appl. Catal. B Environ.* **2021**, *298*, 120583. [\[CrossRef\]](#)
22. Zhong, X.; Zhong, Z.; Liang, S.; Zeng, G.; Cheng, S.; Deng, H.; Lin, Z. Towards a broad-operation window for stable CO<sub>2</sub> electroreduction to HCOOH by a design involving upcycling electroplating sludge-derived Sn@N/P-doped carbon. *Environ. Sci. Nano* **2022**, *9*, 511–522. [\[CrossRef\]](#)
23. Liu, H.; Hu, G.; Luo, Y.; Zhang, K.; Chen, S.; Qin, A. Red mud-based lithium-ion battery anode material with high electrochemical performance prepared by acid and SDS-assisted hydrothermal method. *J. Mater. Sci. Mater. Electron.* **2022**, *33*, 6201–6213. [\[CrossRef\]](#)
24. Zhang, Y.; Chen, M.; Chen, Z.; Wang, Y.; Li, S.; Duan, P.; Zhong, Y.; Wu, Z.; Guo, X.; Yan, Z.; et al. Constructing cycle-stable Si/TiSi<sub>2</sub> composites as anode materials for lithium ion batteries through direct utilization of low-purity Si and Ti-bearing blast furnace slag. *J. Alloys Compd.* **2021**, *876*, 160125. [\[CrossRef\]](#)
25. Weng, C.; Sun, X.; Han, B.; Ye, X.; Zhong, Z.; Li, W.; Liu, W.; Deng, H.; Lin, Z. Targeted conversion of Ni in electroplating sludge to nickel ferrite nanomaterial with stable lithium storage performance. *J. Hazard. Mater.* **2020**, *393*, 122296. [\[CrossRef\]](#)
26. Chun, J.; An, S.; Lee, J. Highly mesoporous silicon derived from waste iron slag for high performance lithium ion battery anodes. *J. Mater. Chem. A* **2015**, *3*, 21899–21906. [\[CrossRef\]](#)
27. Sun, Z.; Hu, Y.; Zeng, K.; Li, M.; Zhao, S.; Zhang, J. Turn “Waste” Into Wealth: MoO<sub>2</sub>@coal Gangue Electrocatalyst with Amorphous/Crystalline Heterostructure for Efficient Li–O<sub>2</sub> Batteries. *Small* **2023**, *19*, 2208145. [\[CrossRef\]](#)
28. Wu, Z.J.; Yue, H.F.; Li, L.S.; Jiang, B.F.; Wu, X.R.; Wang, P. Synthesis and electrochemical properties of multi-doped LiFePO<sub>4</sub>/C prepared from the steel slag. *J. Power Sources* **2010**, *195*, 2888–2893. [\[CrossRef\]](#)
29. Chen, D.; Chen, H.; Du, C.-F.; Liu, L.; Geng, H.; Yu, H.; Rui, X. From vanadium slag to multi-cation-intercalated V<sub>2</sub>O<sub>5</sub>·nH<sub>2</sub>O: Low-cost direct synthesis and high-performance aqueous battery application. *J. Mater. Chem. A* **2022**, *10*, 5479–5487. [\[CrossRef\]](#)
30. Lv, T.; Li, J.; Shi, Y.; Yu, H.; Chen, J. Activating biomass carbon with metallurgical slag by pyrolysis in molten salt for high-performance supercapacitors. *RSC Adv.* **2023**, *13*, 23021–23029. [\[CrossRef\]](#)
31. Shaikh, A.; Singh, B.K.; Purnendu, K.; Kumari, P.; Sankar, P.R.; Mundra, G.; Bohm, S. Utilization of the nickel hydroxide derived from a spent electroless nickel plating bath for energy storage applications. *RSC Sustain.* **2023**, *1*, 294–302. [\[CrossRef\]](#)

32. Xie, Y.; Sun, Z.; Han, T.; Xie, Z.; Zhang, J.; Sun, H.; Xiao, J.; Wang, Y.; Yu, F.; Yang, N. Highly efficient utilization of industrial barium slag for carbon gasification in direct carbon solid oxide fuel cells. *Int. J. Hydrogen Energy* **2021**, *46*, 37029–37038. [\[CrossRef\]](#)
33. Yang, S.; An, H.; Anastasiadou, D.; Xu, W.; Wu, L.; Wang, H.; de Ruiter, J.; Arnouts, S.; Figueiredo, M.C.; Bals, S.; et al. Waste-Derived Copper-Lead Electrocatalysts for CO<sub>2</sub> Reduction. *ChemCatChem* **2022**, *14*, e202200754. [\[CrossRef\]](#) [\[PubMed\]](#)
34. Zhang, Y.; Cui, Y.; Zhang, J.; Xu, Y.; Liu, Q.; Qian, G. Synthesis of electrocatalyst from electroplating sludge for efficient N<sub>2</sub> reduction under ambient conditions. *Chem. Eng. J.* **2022**, *429*, 132357. [\[CrossRef\]](#)
35. Xu, Y.-T.; Ren, K.-C.; Tao, Z.-M.; Sam, D.K.; Feng, E.; Wang, X.; Zhang, G.; Wu, J.; Cao, Y. A new catalyst based on disposed red mud for the efficient electrochemical reduction of nitrate-to-ammonia. *Green Chem.* **2023**, *25*, 589–595. [\[CrossRef\]](#)
36. Chen, Z.; Wei, W.; Ni, B.-J.; Chen, H. Plastic wastes derived carbon materials for green energy and sustainable environmental applications. *Environ. Funct. Mater.* **2022**, *1*, 34–48. [\[CrossRef\]](#)
37. Lv, X.; Tang, F.; Yao, Y.; Xu, C.; Chen, D.; Liu, L.; Feng, Y.; Rui, X.; Yu, Y. Sodium–gallium alloy layer for fast and reversible sodium deposition. *SusMat* **2022**, *2*, 699–707. [\[CrossRef\]](#)
38. Li, Y.; Ma, D.; Wang, Y.; Yang, H.; Lou, Z.; Qin, R.; Zhao, Q.; Pan, F.; Liu, H. A novel bimetallic RuFe nanocluster to enable highly efficient oxygen reduction in zinc-air batteries. *Prog. Nat. Sci. Mater. Int.* **2022**, *32*, 769–775. [\[CrossRef\]](#)
39. Yan, N.-F.; Cui, H.-M.; Shi, J.-S.; You, S.-Y.; Liu, S. Recent progress of W<sub>18</sub>O<sub>49</sub> nanowires for energy conversion and storage. *Tungsten* **2023**. [\[CrossRef\]](#)
40. Fu, Y.; Jin, Y.; Ma, J.; Liu, J.; Wang, Z.; Wang, B.; Gong, X. Lithium-ion transfer strengthened by graphite tailings and coking coal for high-rate performance anode. *Chem. Eng. J.* **2022**, *442*, 136184. [\[CrossRef\]](#)
41. Zhang, L.; Zhu, C.; Yu, S.; Ge, D.; Zhou, H. Status and challenges facing representative anode materials for rechargeable lithium batteries. *J. Energy Chem.* **2022**, *66*, 260–294. [\[CrossRef\]](#)
42. Li, X.; Chen, Y.; Huang, H.; Mai, Y.-W.; Zhou, L. Electrospun carbon-based nanostructured electrodes for advanced energy storage—a review. *Energy Storage Mater.* **2016**, *5*, 58–92. [\[CrossRef\]](#)
43. Hou, L.; Xing, B.; Zeng, H.; Kang, W.; Guo, H.; Cheng, S.; Huang, G.; Cao, Y.; Chen, Z.; Zhang, C. Aluminothermic reduction synthesis of Si/C composite nanosheets from waste vermiculite as high-performance anode materials for lithium-ion batteries. *J. Alloys Compd.* **2022**, *922*, 166134. [\[CrossRef\]](#)
44. Zhang, S.; Zhang, N.; Zhao, W.; Lan, D.; Hao, G.; Yi, X.; Yang, Z.; Hu, J.; He, W.; Liu, Y.; et al. Green preparation of hierarchical porous C/SiO<sub>x</sub> composites from coal gangue as anodes for Li-ion batteries. *Solid State Ion.* **2021**, *371*, 115772. [\[CrossRef\]](#)
45. Idota, Y.; Kubota, T.; Matsufuji, A.; Maekawa, Y.; Miyasaka, T. Tin-based amorphous oxide: A high-capacity lithium-ion-storage material. *Science* **1997**, *276*, 1395–1397. [\[CrossRef\]](#)
46. Ye, X.; Lin, Z.; Liang, S.; Huang, X.; Qiu, X.; Qiu, Y.; Liu, X.; Xie, D.; Deng, H.; Xiong, X.; et al. Upcycling of Electroplating Sludge into Ultrafine Sn@C Nanorods with Highly Stable Lithium Storage Performance. *Nano Lett.* **2019**, *19*, 1860–1866. [\[CrossRef\]](#) [\[PubMed\]](#)
47. Zheng, M.; Tang, H.; Li, L.; Hu, Q.; Zhang, L.; Xue, H.; Pang, H. Hierarchically nanostructured transition metal oxides for lithium-ion batteries. *Adv. Sci.* **2018**, *5*, 1700592. [\[CrossRef\]](#) [\[PubMed\]](#)
48. Chen, Z.; Wei, W.; Chen, H.; Ni, B.-J. Eco-designed electrocatalysts for water splitting: A path toward carbon neutrality. *Int. J. Hydrogen Energy* **2023**, *48*, 6288–6307. [\[CrossRef\]](#)
49. Suryawanshi, A.; Aravindan, V.; Madhavi, S.; Ogale, S. Red Mud and Li-Ion Batteries: A Magnetic Connection. *ChemSusChem* **2016**, *9*, 2193–2200. [\[CrossRef\]](#)
50. Zhang, Y.; Ma, C.; He, W.; Zhang, C.; Zhou, L.; Wang, G.; Wei, W. MXene and MXene-based materials for lithium-sulfur batteries. *Prog. Nat. Sci. Mater. Int.* **2021**, *31*, 501–513. [\[CrossRef\]](#)
51. Zou, W.; Li, J.; Wang, R.; Ma, J.; Chen, Z.; Duan, L.; Mi, H.; Chen, H. Hydroxylamine mediated Fenton-like interfacial reaction dynamics on sea urchin-like catalyst derived from spent LiFePO<sub>4</sub> battery. *J. Hazard. Mater.* **2022**, *431*, 128590. [\[CrossRef\]](#)
52. Guo, J.; Feng, Y.; Mo, X.; Liao, G. Preparation of LiFePO<sub>4</sub> using iron(II) sulfate as product from titanium dioxide slag purification process and its electrochemical properties. *Int. J. Electrochem. Sci.* **2021**, *16*, 211141. [\[CrossRef\]](#)
53. Kang, H.; Wang, G.; Guo, H.; Chen, M.; Luo, C.; Yan, K. Facile Synthesis and Electrochemical Performance of LiFePO<sub>4</sub>/C Composites Using Fe–P Waste Slag. *Ind. Eng. Chem. Res.* **2012**, *51*, 7923–7931. [\[CrossRef\]](#)
54. Lan, D.; Zhang, G.; Mo, M.; Fang, Z.; Shi, S.; Hu, K.; Huang, Y.; Zang, R.; Li, W.; Zhan, H.; et al. Short-process simultaneously recycling cobalt and manganese from environment-hazardous di-methyl-dithiocarbamate chelate slag as lithium-ion battery cathode material. *Sustain. Energy Technol. Assess.* **2023**, *57*, 103231. [\[CrossRef\]](#)
55. Meng, X.; Cao, H.; Hao, J.; Ning, P.; Xu, G.; Sun, Z. Sustainable Preparation of LiNi<sub>1/3</sub>Co<sub>1/3</sub>Mn<sub>1/3</sub>O<sub>2</sub>–V<sub>2</sub>O<sub>5</sub> Cathode Materials by Recycling Waste Materials of Spent Lithium-Ion Battery and Vanadium-Bearing Slag. *ACS Sustain. Chem. Eng.* **2018**, *6*, 5797–5805. [\[CrossRef\]](#)
56. Wu, L.; Li, X.-H.; Wang, Z.-X.; Li, L.-J.; Zheng, J.-C.; Guo, H.-J.; Hu, Q.-Y.; Fang, J. Synthesis and electrochemical properties of metals-doped LiFePO<sub>4</sub> prepared from the FeSO<sub>4</sub>·7H<sub>2</sub>O waste slag. *J. Power Sources* **2009**, *189*, 681–684. [\[CrossRef\]](#)
57. Wu, L.; Wang, Z.; Li, X.; Guo, H.; Li, L.; Wang, X.; Zheng, J. Cation-substituted LiFePO<sub>4</sub> prepared from the FeSO<sub>4</sub>·7H<sub>2</sub>O waste slag as a potential Li battery cathode material. *J. Alloys Compd.* **2010**, *497*, 278–284. [\[CrossRef\]](#)
58. Li, P.; Luo, S.-H.; Wang, J.; Wang, Y.; Wang, Q.; Zhang, Y.; Liu, X.; Gao, D.; Lv, F.; Mu, W.; et al. Extraction and separation of Fe and Ti from extracted vanadium residue by enhanced ammonium sulfate leaching and synthesis of LiFePO<sub>4</sub>/C for lithium-ion batteries. *Sep. Purif. Technol.* **2022**, *282*, 120065. [\[CrossRef\]](#)

59. Yang, L.; Feng, Y.; Wang, C.; Fang, D.; Yi, G.; Gao, Z.; Shao, P.; Liu, C.; Luo, X.; Luo, S. Closed-loop regeneration of battery-grade  $\text{FePO}_4$  from lithium extraction slag of spent Li-ion batteries via phosphoric acid mixture selective leaching. *Chem. Eng. J.* **2022**, *431*, 133232. [\[CrossRef\]](#)
60. Lv, T.; Peng, Y.; Zhang, G.; Jiang, S.; Yang, Z.; Yang, S.; Pang, H. How About Vanadium-Based Compounds as Cathode Materials for Aqueous Zinc Ion Batteries? *Adv. Sci.* **2023**, *10*, 2206907. [\[CrossRef\]](#)
61. Xu, G.; Liu, X.; Huang, S.; Li, L.; Wei, X.; Cao, J.; Yang, L.; Chu, P.K. Freestanding; Hierarchical, and Porous Bilayered  $\text{Na}_x\text{V}_2\text{O}_5 \cdot n\text{H}_2\text{O}/\text{rGO}/\text{CNT}$  Composites as High-Performance Cathode Materials for Nonaqueous K-Ion Batteries and Aqueous Zinc-Ion Batteries. *ACS Appl. Mater. Interfaces* **2019**, *12*, 706–716. [\[CrossRef\]](#)
62. Hua, W.; Li, H.; Pei, C.; Xia, J.; Sun, Y.; Zhang, C.; Lv, W.; Tao, Y.; Jiao, Y.; Zhang, B. Selective catalysis remedies polysulfide shuttling in lithium-sulfur batteries. *Adv. Mater.* **2021**, *33*, 2101006. [\[CrossRef\]](#) [\[PubMed\]](#)
63. Wu, S.; Ke, Y.; Tang, J.; Lei, X.; Deng, H.; Lin, Z. Upcycling of electroplating sludge into  $\text{Fe}_3\text{C}$ -decorated N,P dual-doped porous carbon via microalgae as efficient sulfur host for lithium-sulfur batteries. *Surf. Interfaces* **2022**, *30*, 101869. [\[CrossRef\]](#)
64. Kwak, W.-J.; Rosy; Sharon, D.; Xia, C.; Kim, H.; Johnson, L.R.; Bruce, P.G.; Nazar, L.F.; Sun, Y.-K.; Frimer, A.A.; et al. Lithium-Oxygen Batteries and Related Systems: Potential, Status, and Future. *Chem. Rev.* **2020**, *120*, 6626–6683. [\[CrossRef\]](#)
65. Sun, Z.; Zhou, N.; Li, M.; Xu, J.; Feng, W.; Liu, S. Functional Control Engineering of Coal Gangue Electrocatalyst with Amorphous  $\text{SiCX}/\text{SiOX}$  Active Layer Loading Enables Efficient  $\text{Li-O}_2$  Batteries. *Appl. Sci.* **2023**, *13*, 5551. [\[CrossRef\]](#)
66. Zhao, J.; Burke, A.F. Review on supercapacitors: Technologies and performance evaluation. *J. Energy Chem.* **2021**, *59*, 276–291. [\[CrossRef\]](#)
67. Liu, W.-J.; Yuan, M.; Lian, J.-B.; Li, G.-C.; Li, Q.-P.; Qiao, F.; Zhao, Y. Embedding partial sulfurization of iron-cobalt oxide nanoparticles into carbon nanofibers as an efficient electrode for the advanced asymmetric supercapacitor. *Tungsten* **2023**, *5*, 118–129. [\[CrossRef\]](#)
68. Chen, Z.; Wei, W.; Ni, B.-J. Cost-effective catalysts for renewable hydrogen production via electrochemical water splitting: Recent advances. *Curr. Opin. Green Sustain. Chem.* **2021**, *27*, 100398. [\[CrossRef\]](#)
69. Bhattacharya, G.; Fishlock, S.J.; Roy, J.S.; Pritam, A.; Banerjee, D.; Deshmukh, S.; Ghosh, S.; McLaughlin, J.A.; Roy, S.S. Effective Utilization of Waste Red Mud for High Performance Supercapacitor Electrodes. *Glob. Chall.* **2019**, *3*, 1800066. [\[CrossRef\]](#)
70. Yadav, P.; Raju, M.K.; Samudrala, R.K.; Gangadhar, M.; Pani, J.; Borkar, H.; Azeem, P.A. Cost-effective akermanite derived from industrial waste for working electrodes in supercapacitor applications. *New J. Chem.* **2023**, *47*, 3255–3265. [\[CrossRef\]](#)
71. Liu, T.; Zhou, H.; Zhong, G.; Yan, X.; Su, X.; Lin, Z. Synthesis of  $\text{NiFeAl}$  LDHs from electroplating sludge and Their excellent supercapacitor performance. *J. Hazard. Mater.* **2021**, *404*, 124113. [\[CrossRef\]](#) [\[PubMed\]](#)
72. Zhan, P.; Xu, J.; Wang, J.; Zuo, J.; He, Z. Structural supercapacitor electrolytes based on cementitious composites containing recycled steel slag and waste glass powders. *Cem. Concr. Compos.* **2023**, *137*, 104924. [\[CrossRef\]](#)
73. Zeng, C.; Duan, C.; Guo, Z.; Liu, Z.; Dou, S.; Yuan, Q.; Liu, P.; Zhang, J.; Luo, J.; Liu, W.; et al. Ultrafastly activated needle coke as electrode material for supercapacitors. *Prog. Nat. Sci. Mater. Int.* **2022**, *32*, 786–792. [\[CrossRef\]](#)
74. Muthukannan, V.; Praveen, K.; Natesan, B. Fabrication and characterization of magnetite/reduced graphene oxide composite incurred from iron ore tailings for high performance application. *Mater. Chem. Phys.* **2015**, *162*, 400–407. [\[CrossRef\]](#)
75. Livinus, O.C.; Sochima, E.V.; Joy, E.N.; Aigbodion, V.S. Insights in the synthesis and electrochemical performance of tin tailings/graphene derived from rice husk/polyester composite electrode materials for supercapacitors. *Int. J. Adv. Manuf. Technol.* **2023**, *128*, 1879–1888. [\[CrossRef\]](#)
76. Bhattacharya, G.; Fishlock, S.J.; Pritam, A.; Roy, S.S.; McLaughlin, J.A. Recycled Red Mud-Decorated Porous 3D Graphene for High-Energy Flexible Micro-Supercapacitor. *Adv. Sustain. Syst.* **2020**, *4*, 1900133. [\[CrossRef\]](#)
77. Chen, Z.; Wei, W.; Chen, H.; Ni, B. Recent advances in waste-derived functional materials for wastewater remediation. *Eco-Environ. Health* **2022**, *1*, 86–104. [\[CrossRef\]](#)
78. Li, Y.; Han, X.; Yi, T.; He, Y.; Li, X. Review and prospect of  $\text{NiCo}_2\text{O}_4$ -based composite materials for supercapacitor electrodes. *J. Energy Chem.* **2019**, *31*, 54–78. [\[CrossRef\]](#)
79. Hou, Z.; Liu, T.; Tahir, M.U.; Ahmad, S.; Shao, X.; Yang, C.; He, B.; Su, X. Facile conversion of nickel-containing electroplating sludge into nickel-based multilevel nano-material for high-performance pseudocapacitors. *Appl. Surf. Sci.* **2021**, *538*, 147978. [\[CrossRef\]](#)
80. Wan, Z.; Tao, Y.; Shao, J.; Zhang, Y.; You, H. Ammonia as an effective hydrogen carrier and a clean fuel for solid oxide fuel cells. *Energy Convers. Manag.* **2021**, *228*, 113729. [\[CrossRef\]](#)
81. Graś, M.; Kolanowski, Ł.; Chen, Z.; Lota, K.; Jurak, K.; Ryl, J.; Ni, B.-J.; Lota, G. Partial inhibition of borohydride hydrolysis using porous activated carbon as an effective method to improve the electrocatalytic activity of the DBFC anode. *Sustain. Energy Fuels* **2021**, *5*, 4401–4413. [\[CrossRef\]](#)
82. Glibin, V.P.; Dodelet, J.-P.; Zhang, G. Energetics and thermodynamic stability of potential  $\text{Fe(II)}$ -hexa-aza-active sites for  $\text{O}_2$  reduction in PEM fuel cells. *SusMat* **2022**, *2*, 731–748. [\[CrossRef\]](#)
83. Han, T.; Wu, Y.; Xie, Z.; Li, L.; Wang, Y.; Xie, Y.; Zhang, J.; Xiao, J.; Yu, F.; Yang, N. A novel Boudouard reaction catalyst derived from strontium slag for enhanced performance of direct carbon solid oxide fuel cells. *J. Alloys Compd.* **2022**, *895*, 162643. [\[CrossRef\]](#)
84. Murmu, R.; Roy, D.; Patra, S.C.; Sutar, H.; Choudhary, B. Preparation and Characterization of Red Mud Modified Chitosan-PVA Composite Membrane for Direct Methanol Fuel Cell. *J. Electrochem. Energy Convers. Storage* **2023**, *20*, 031008. [\[CrossRef\]](#)

85. Kim, K.; Nakashita, S.; Hibino, T. Enhanced power performance of an in situ sediment microbial fuel cell with steel-slag as the redox catalyst: I. electricity generation. *Sustain. Energy Fuels* **2020**, *4*, 1363–1371. [\[CrossRef\]](#)
86. Jiang, C.; Ma, J.; Corre, G.; Jain, S.L.; Irvine, J.T. Challenges in developing direct carbon fuel cells. *Chem. Soc. Rev.* **2017**, *46*, 2889–2912. [\[CrossRef\]](#) [\[PubMed\]](#)
87. Jiao, Y.; Wang, C.; Zhang, L.; An, W.; Zhou, N.; Yang, G.; Wang, W.; Zhou, W.; Li, S.-D. A steel slag-derived Boudouard reaction catalyst for improved performance of direct carbon solid oxide fuel cells. *Int. J. Energy Res.* **2019**, *43*, 6970–6982. [\[CrossRef\]](#)
88. Yaqoob, A.A.; Ibrahim, M.N.M.; Yaakop, A.S.; Umar, K.; Ahmad, A. Modified graphene oxide anode: A bioinspired waste material for bioremediation of Pb<sup>2+</sup> with energy generation through microbial fuel cells. *Chem. Eng. J.* **2021**, *417*, 128052. [\[CrossRef\]](#)
89. Chen, Z.; Han, N.; Zheng, R.; Ren, Z.; Wei, W.; Ni, B.J. Design of earth-abundant amorphous transition metal-based catalysts for electrooxidation of small molecules: Advances and perspectives. *SusMat* **2023**, *3*, 290–319. [\[CrossRef\]](#)
90. Du, C.; Qiu, C.; Fang, Z.; Li, P.; Gao, Y.; Wang, J.; Chen, W. Interface hydrophobic tunnel engineering: A general strategy to boost electrochemical conversion of N<sub>2</sub> to NH<sub>3</sub>. *Nano Energy* **2022**, *92*, 106784. [\[CrossRef\]](#)
91. Rossi, K.; Buonsanti, R. Shaping copper nanocatalysts to steer selectivity in the electrochemical CO<sub>2</sub> reduction reaction. *Acc. Chem. Res.* **2022**, *55*, 629–637. [\[CrossRef\]](#)
92. Han, N.; Feng, S.; Guo, W.; Mora, O.M.; Zhao, X.; Zhang, W.; Xie, S.; Zhou, Z.; Liu, Z.; Liu, Q. Rational design of Ruddlesden–Popper perovskite electrocatalyst for oxygen reduction to hydrogen peroxide. *SusMat* **2022**, *2*, 456–465. [\[CrossRef\]](#)
93. Chen, Z.; Zheng, R.; Zou, H.; Wang, R.; Huang, C.; Dai, W.; Wei, W.; Duan, L.; Ni, B.-J.; Chen, H. Amorphous Iron-doped Nickel Boride with Facilitated Structural Reconstruction and Dual Active Sites for Efficient Urea Electrooxidation. *Chem. Eng. J.* **2023**, *465*, 142684. [\[CrossRef\]](#)
94. Zheng, D.; Li, J.; Ci, S.; Cai, P.; Ding, Y.; Zhang, M.; Wen, Z. Three-birds-with-one-stone electrolysis for energy-efficiency production of gluconate and hydrogen. *Appl. Catal. B Environ.* **2020**, *277*, 119178. [\[CrossRef\]](#)
95. Luo, Y.; Zhang, Z.; Yang, F.; Li, J.; Liu, Z.; Ren, W.; Zhang, S.; Liu, B. Stabilized hydroxide-mediated nickel-based electrocatalysts for high-current-density hydrogen evolution in alkaline media. *Energy Environ. Sci.* **2021**, *14*, 4610–4619. [\[CrossRef\]](#)
96. Zhao, H.; Zhang, Y.; Zhao, B.; Chang, Y.; Li, Z. Electrochemical reduction of carbon dioxide in an MFC–MEC system with a layer-by-layer self-assembly carbon nanotube/cobalt phthalocyanine modified electrode. *Environ. Sci. Technol.* **2012**, *46*, 5198–5204. [\[CrossRef\]](#)
97. Yuan, H.; Deng, L.; Cai, X.; Zheng, T.; Zhou, S.; Chen, Y.; Yuan, Y. Recycling electroplating sludge to produce sustainable electrocatalysts for the efficient conversion of carbon dioxide in a microbial electrolysis cell. *Electrochim. Acta* **2016**, *222*, 177–184. [\[CrossRef\]](#)
98. Li, C.; Ding, S.; Zhang, J.; Wu, J.; Yue, Y.; Qian, G. Ball milling transformed electroplating sludges with different components to spinels for stable electrocatalytic ammonia production under ambient conditions. *Chemosphere* **2022**, *296*, 134060. [\[CrossRef\]](#)
99. Chen, G.-F.; Yuan, Y.; Jiang, H.; Ren, S.-Y.; Ding, L.-X.; Ma, L.; Wu, T.; Lu, J.; Wang, H. Electrochemical reduction of nitrate to ammonia via direct eight-electron transfer using a copper–molecular solid catalyst. *Nat. Energy* **2020**, *5*, 605–613. [\[CrossRef\]](#)
100. Chen, Z.; Wei, W.; Shen, Y.; Ni, B.-J. Defective nickel sulfide hierarchical structures for efficient electrochemical conversion of plastic waste to value-added chemicals and hydrogen fuel. *Green Chem.* **2023**, *25*, 5979–5988. [\[CrossRef\]](#)
101. Dai, W.; Wang, R.; Chen, Z.; Deng, S.; Huang, C.; Luo, W.; Chen, H. Highly-efficient photocatalytic hydrogen evolution triggered by spatial confinement effects over co-crystal templated boron-doped carbon nitride hollow nanotubes. *J. Mater. Chem. A* **2023**, *11*, 7584–7595. [\[CrossRef\]](#)
102. Li, X.-X.; Liu, X.-C.; Liu, C.; Zeng, J.-M.; Qi, X.-P. Co<sub>3</sub>O<sub>4</sub>/stainless steel catalyst with synergistic effect of oxygen vacancies and phosphorus doping for overall water splitting. *Tungsten* **2023**, *5*, 100–108. [\[CrossRef\]](#)
103. Zhang, L.; Zhao, H.; Xu, S.; Liu, Q.; Li, T.; Luo, Y.; Gao, S.; Shi, X.; Asiri, A.M.; Sun, X. Recent Advances in 1D Electrospun Nanocatalysts for Electrochemical Water Splitting. *Small Struct.* **2021**, *2*, 2000048. [\[CrossRef\]](#)
104. Han, N.; Zhang, W.; Guo, W.; Pan, H.; Jiang, B.; Xing, L.; Tian, H.; Wang, G.; Zhang, X.; Fransaer, J. Designing Oxide Catalysts for Oxygen Electrocatalysis: Insights from Mechanism to Application. *Nano-Micro Lett.* **2023**, *15*, 185. [\[CrossRef\]](#) [\[PubMed\]](#)
105. Wang, Y.; Tao, S.; Lin, H.; Wang, G.; Zhao, K.; Cai, R.; Tao, K.; Zhang, C.; Sun, M.; Hu, J.; et al. Atomically targeting NiFe LDH to create multivacancies for OER catalysis with a small organic anchor. *Nano Energy* **2021**, *81*, 105606. [\[CrossRef\]](#)
106. Han, N.; Feng, S.; Liang, Y.; Wang, J.; Zhang, W.; Guo, X.; Ma, Q.; Liu, Q.; Guo, W.; Zhou, Z.; et al. Achieving Efficient Electrocatalytic Oxygen Evolution in Acidic Media on Yttrium Ruthenate Pyrochlore through Cobalt Incorporation. *Adv. Funct. Mater.* **2023**, *33*, 2208399. [\[CrossRef\]](#)
107. Chen, Z.; Zheng, R.; Wei, W.; Wei, W.; Zou, W.; Li, J.; Ni, B.-J.; Chen, H. Recycling spent water treatment adsorbents for efficient electrocatalytic water oxidation reaction. *Resour. Conserv. Recycl.* **2022**, *178*, 106037. [\[CrossRef\]](#)
108. Zhang, L.; Li, L.; Liang, J.; Fan, X.; He, X.; Chen, J.; Li, J.; Li, Z.; Cai, Z.; Sun, S. Highly efficient and stable oxygen evolution from seawater enabled by a hierarchical NiMoS<sub>x</sub> microcolumn@NiFe-layered double hydroxide nanosheet array. *Inorg. Chem. Front.* **2023**, *10*, 2766–2775. [\[CrossRef\]](#)
109. Kim, M.; Kim, J.; Qin, L.; Mathew, S.; Han, Y.; Li, O.L. Gas-Liquid Interfacial Plasma engineering under dilute nitric acid to improve hydrophilicity and OER performance of nickel foam. *Prog. Nat. Sci. Mater. Int.* **2022**, *32*, 608–616. [\[CrossRef\]](#)
110. Chen, Z.; Zou, W.; Zheng, R.; Wei, W.; Wei, W.; Ni, B.-J.; Chen, H. Synergistic recycling and conversion of spent Li-ion battery leachate into highly efficient oxygen evolution catalysts. *Green Chem.* **2021**, *23*, 6538–6547. [\[CrossRef\]](#)

111. Chen, Z.; Wei, W.; Zou, W.; Li, J.; Zheng, R.; Wei, W.; Ni, B.-J.; Chen, H. Integrating electrodeposition with electrolysis for closing loop resource utilization of battery industrial wastewater. *Green Chem.* **2022**, *44*, 3208–3217. [[CrossRef](#)]
112. Chi, H.; Wang, J.; Wang, H.; Li, S.; Yang, M.; Bai, S.; Li, C.; Sun, X.; Zhao, Y.; Song, Y.-F. Super-Stable Mineralization of Ni<sup>2+</sup> Ions from Wastewater using CaFe Layered Double Hydroxide. *Adv. Funct. Mater.* **2022**, *32*, 2106645. [[CrossRef](#)]

**Disclaimer/Publisher’s Note:** The statements, opinions and data contained in all publications are solely those of the individual author(s) and contributor(s) and not of MDPI and/or the editor(s). MDPI and/or the editor(s) disclaim responsibility for any injury to people or property resulting from any ideas, methods, instructions or products referred to in the content.